DEC 09 2003

0830-L-02 NAS1.29/3-2:02-12

NASA Tech Briefs

National Aeronautics and
Space Administration

Electronic Components and Circuits

Electronic Systems

Physical Sciences

Materials

Computer Programs

Mechanics

Machinery

Fabrication Technology

Mathematics and Information Sciences

Life Sciences

20040101 10 AM

INTRODUCTION

Tech Briefs are short announcements of innovations originating from research and development activities of the National Aeronautics and Space Administration. They emphasize information considered likely to be transferable across industrial, regional, or disciplinary lines and are issued to encourage commercial application.

Availability of NASA Tech Briefs and TSPs

Requests for individual Tech Briefs or for Technical Support Packages (TSPs) announced herein should be addressed to

National Technology Transfer Center
Telephone No. **(800) 678-6882** or via World Wide Web at **www2.nttc.edu/leads/**

Please reference the control numbers appearing at the end of each Tech Brief. Information on NASA's Commercial Technology Team, its documents, and services is also available at the same facility or on the World Wide Web at **www.nctn.hq.nasa.gov**.

Commercial Technology Offices and Patent Counsels are located at NASA field centers to provide technology-transfer access to industrial users. Inquiries can be made by contacting NASA field centers and program offices listed below.

NASA Field Centers and Program Offices

Ames Research Center
Carolina Blake
(650) 604-1754 or
cblake@mail.arc.nasa.gov

Dryden Flight Research Center
Jenny Baer-Riedhart
(661) 276-3689 or
jenny.baer-riedhart@dfrc.nasa.gov

Goddard Space Flight Center
Nona Cheeks
(301) 286-5810 or
nona.k.cheeks@gsfc.nasa.gov

Jet Propulsion Laboratory
Merle McKenzie
(818) 354-2577 or
merle.mckenzie@jpl.nasa.gov

Johnson Space Center
Charlene E. Gilbert
(281) 483-3809 or
commercialization@jsc.nasa.gov

John F. Kennedy Space Center
Jim Aliberti
(321) 867-6224 or
Jim.Aliberti-1@ksc.nasa.gov

Langley Research Center
Sam Morello
(757) 864-6005 or
s.a.morello@larc.nasa.gov

Glenn Research Center
Larry Viterna
(216) 433-3484 or
cto@grc.nasa.gov

George C. Marshall Space Flight Center
Vernotto McMillan
(256) 544-2615 or
vernotto.mcmillan@msfc.nasa.gov

John C. Stennis Space Center
Kirk Sharp
(228) 688-1929 or
technology@ssc.nasa.gov

NASA Program Offices
At NASA Headquarters there are seven major program offices that develop and oversee technology projects of potential interest to industry:

Carl Ray
Small Business Innovation Research Program (SBIR) & Small Business Technology Transfer Program (STTR)
(202) 358-4652 or
cray@mail.hq.nasa.gov

Dr. Robert Norwood
Office of Commercial Technology (Code RW)
(202) 358-2320 or
rnorwood@mail.hq.nasa.gov

John Mankins
Office of Space Flight (Code MP)
(202) 358-4659 or
jmankins@mail.hq.nasa.gov

Terry Hertz
Office of Aero-Space Technology (Code RS)
(202) 358-4636 or
thertz@mail.hq.nasa.gov

Glen Mucklow
Office of Space Sciences (Code SM)
(202) 358-2235 or
gmucklow@mail.hq.nasa.gov

Roger Crouch
Office of Microgravity Science Applications (Code U)
(202) 358-0689 or
rcrouch@hq.nasa.gov

Granville Paules
Office of Mission to Planet Earth (Code Y)
(202) 358-0706 or
gpaules@mtpe.hq.nasa.gov

TechBriefs

National Aeronautics and
Space Administration

December 2002
02-12

5	**Electronic Components and Circuits**	
11	**Electronic Systems**	
17	**Physical Sciences**	
23	**Materials**	
27	**Computer Programs**	
31	**Mechanics**	
37	**Machinery**	
41	**Fabrication Technology**	
45	**Mathematics and Information Sciences**	

This document was prepared under the sponsorship of the National Aeronautics and Space Administration. Neither the United States Government nor any person acting on behalf of the United States Government assumes any liability resulting from the use of the information contained in this document, or warrants that such use will be free from privately owned rights.

4

BLANK PAGE

Electronic Components and Circuits

Hardware, Techniques, and Processes

7 Data Acquisition and Control Systems Laboratory

7 Geography-Based Routing in an Ad Hoc Communication Network

8 Photodiode CMOS Imager With Column Feedback Soft Reset

BLANK PAGE

Data Acquisition and Control Systems Laboratory

Data-acquisition and control systems can now be developed without interfering with on-going test operations.

Stennis Space Center, Mississippi

The Data Acquisition and Control Systems (DACS) Laboratory is a facility at Stennis Space Center that provides an off test-stand capability to develop data-acquisition and control systems for rocket-engine test stands. It is also used to train new employees in state-of-the-art systems, and provides a controlled environment for troubleshooting existing systems, as well as the ability to evaluate the application of new technologies and process improvements. With the SSC propulsion testing schedule, without the DACS Laboratory, it would have been necessary to perform most of the development work on actual test systems, thereby subjecting both the rocket-engine testing and development programs to substantial interference in the form of delays, restrictions on modifications of equipment, and potentially compromising software configuration control. The DACS Laboratory contains a versatile assortment of computer hardware and software, digital and analog electronic control and data-acquisition equipment, and standard electronic bench test equipment and tools (see figure).

Recently completed Control System development and software verification projects include support to the joint NASA/Air Force Integrated Powerhead Demonstration (IPD) LOX & LH2 PreBurner and Turbopump ground testing programs.

In other recent activities, the DACS Laboratory equipment and expertise have supported the off-stand operation of high-pressure control valves to correct valve leak problems prior to installation on the test stand.

Future plans include expanding the Laboratory's capabilities to provide cryogenic control valve characterization prior to installation, thereby reducing test stand activation time.

This work was done by Randy Holland and Scott Jensen of **Stennis Space Center** *and Terrence Burrel and Richard Spooner of Lockheed Martin Corp.*
SSC-00162

This Workstation, which is part of the DACS Laboratory, is dedicated to the development and testing of control systems.

Geography-Based Routing in an Ad Hoc Communication Network

This adaptive algorithm does not require detailed knowledge of network resources.

NASA's Jet Propulsion Laboratory, Pasadena, California

The best-effort geographical multi-hop routing (BEGHR) protocol routes packets of data in an *ad hoc* digital radio-communication network on the basis of the current geographical positions of all the network nodes. This protocol was conceived especially for application to a network, (1) the nodes of which are equipped with Global Positioning System receivers to determine their positions, (2) the nodes of which contain environmental sensors, and (3) the main purpose of which is to collect sensory data and relay them to a central node designated as home.

Unlike prior routing algorithms characterized as table-driven, the BEGHR algorithm does not require the maintenance of a routing table containing up-to-date information on the route(s) from every node to every other node. Unlike prior algorithms characterized as on-demand, the BEGHR does not require the discovery of a route from a specific source node to a specific destination node and the subsequent maintenance of that specific route until the route is no longer needed or no longer accessible. Instead, in the BEGHR algorithm, each packet is forwarded on the basis of (1) only minimal local knowledge of network resources, (2) an effort by nodes participating in the hop to adapt toward current optimal forwarding conditions, and (3) statistical measures of performance.

It is assumed that the network is a member of the class of statistically accurate sensor networks (SASNs), defined as networks capable of representing the distributed information gathered by its sensors with a degree of accuracy and timeliness characterized by a statistical measure denoted as currency or currentness: Let $\delta(i)$ be the interval of time between the generation of the ith piece of information and its arrival at home. The source node or the network is said to be (α,β) current if α is the probability that each piece of information arrives within $\delta(i) < \beta$.

Hence, in an SASN, it is sufficient that only some of the data collected by, and transmitted from, all of the nodes reach home in order to represent the collected measurement data to within a specified degree of accuracy and timeliness. Another measure of performance of node or of the network is that of throughput, defined here as (the total number of packets arrived up to a given time) divided by (the number of packets generated up to that time). A throughput <1 could signify that packets had been lost on account of bit errors in noisy transmission channels and/or overflow of queues of packets awaiting transmission.

In the BEGHR, the network nodes are

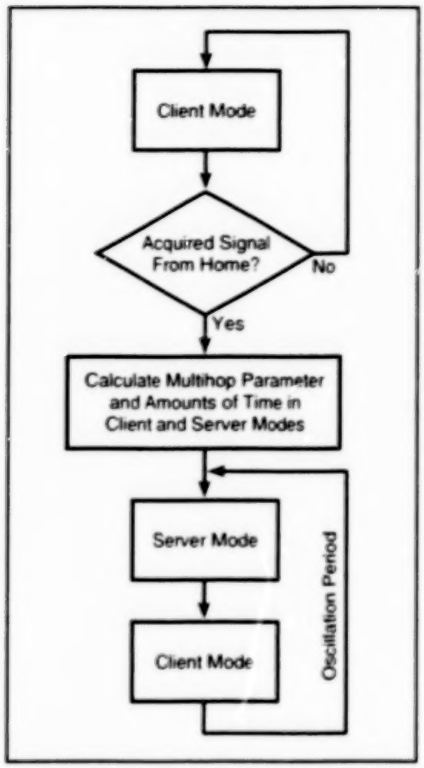

A Network Node Oscillates between client and server modes of operation. A subalgorithm of the BEGHR algorithm allocates portions of the oscillation period to the two modes.

assumed to be randomly positioned. The nodes are also assumed to be identical and each node to be capable of adapting within the network according to its position relative to home and to other nodes that, like itself, are attempting to send data packets to home. Each node is capable of operating in a client mode, defined here as the mode in which it forwards packets, including both those that it generates and those that it received from one or more other node(s) for relay to home. Each node is also capable of operating in a server mode, defined here as the mode in which it receives packets from one or more other nodes. The position of a node relative to home is used to determine whether a packet is in a loop or is being handed off to a node closer to home. Error checking is performed, but acknowledgements are not sent back to originating or relaying nodes, and there is no guarantee that a server node has properly received a packet forwarded from a client node.

Each node oscillates between the client and server modes, dynamically adjusting the time allocated to each mode (see figure). In addition, each node allocates a fixed amount of time to its own local collection of sensory data. The probability of finding the node in one mode or the other depends on its geographical position relative to home. For this purpose, the distance from home is expressed as the multihop parameter of the node, defined as the ratio between (1) its geographical distance from home and (2) the radio-reception distance beyond which the probability of bit error exceeds a value defined in a controlled test scenario. A node located closer to home adapts toward statistically allocating more time as a server, while a sensor located farther from home adapts toward statistically allocating more time as a client. Prior to entering the oscillation, a node waits for home to broadcast (and for any intervening nodes to relay) a message stating the current location of home. Once it goes into the oscillation, the node also relays the home-location message to nodes farther from home.

This work was done by Clayton Okino of Caltech and Michael Corr of Dartmouth College for **NASA's Jet Propulsion Laboratory**. *For further information, access the Technical Support Package (TSP)* ***free on-line at www.nasatech.com***.

This software is available for commercial licensing. Please contact Don Hart of the California Institute of Technology at (818) 393-3425. Refer to NPO-30454.

Photodiode CMOS Imager With Column Feedback Soft Reset

This imager would have a wide dynamic range and would function at ultralow illumination.

NASA's Jet Propulsion Laboratory, Pasadena, California

A proposed complementary metal oxide/semiconductor (CMOS) photodiode integrated-circuit imaging device of the active-pixel-sensor (APS) type would include column feedback sub-circuits that would make it possible to reduce readout noise (thereby making it possible to image at lower light levels) without reducing (and possibly even increasing) full-well capacity (thereby making it possible to obtain wide dynamic range). Heretofore, as described below, low-noise design requirements have generally conflicted with wide-dynamic-range design requirements.

To increase the quality of imaging at low illumination, one must increase quantum efficiency while reducing readout noise. To obtain wide dynamic range (necessary for imaging a high-contrast scene), one must increase the full-well capacity (the number of electrons that each pixel can hold without saturating and overflowing). Unfortunately, a major component of the readout noise of a photodiode APS is the sensing-node reset noise, which is given

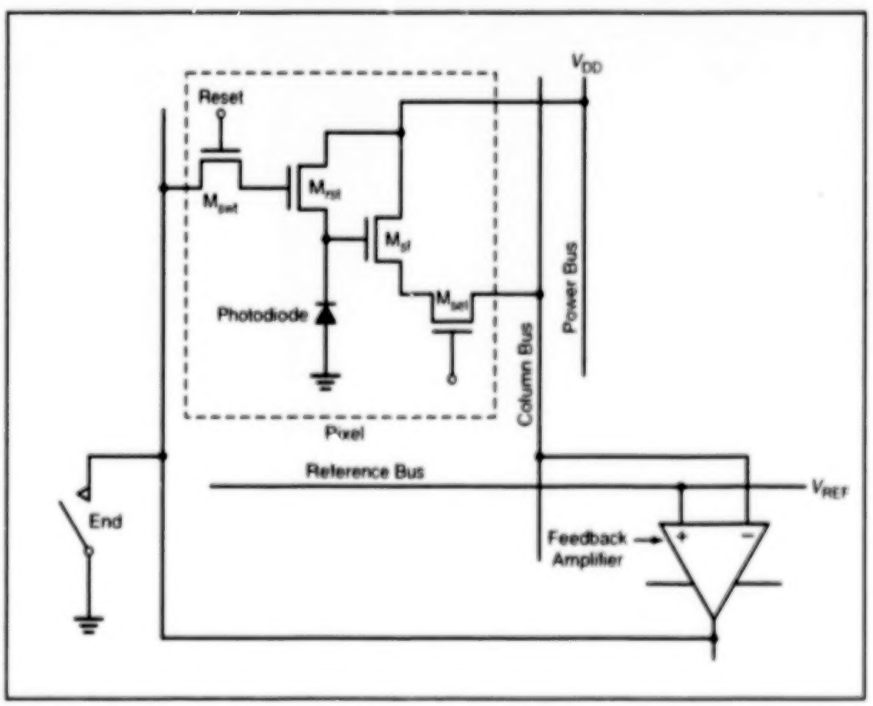

Soft Reset With Column Feedback is the key to low noise and wide dynamic range in this proposed circuit.

by $(kTC_S)^{1/2}/q$, where k is Boltzmann's constant, T is the absolute temperature, C_S is the sensing-node capacitance, and q is the electronic charge. Also unfortunately, in order to increase the full-well capacity, it is necessary to increase C_S. As a result, heretofore, the requirement for low noise (which translates to a requirement for low C_S) has conflicted with the requirement for large full-well capacity (and thus large C_S).

The proposed circuit (see figure) would implement a soft-reset scheme in which the pixels in a given column would be reset to a level determined by column feedback. (In soft reset, both the drain and the gate of an n-channel reset transistor are kept at the same potential.) Each pixel would contain three field-effect transistors (FETs) [M_{sf}, M_{sel}, M_{rst}] that would be conventional for an APS pixel. There would be an unconventional additional FET (M_{bias}) and an additional conductive line, which would be the feedback bus for setting the reset high level.

The feedback for a given column would be processed through a column feedback amplifier, which would strive to minimize the difference between the potential on the column bus and the potential on a reference bus. The reference bus would be common to all columns and would be held at a fixed dc level, V_{REF}. Under feedback, the potential on the gate of M_{rst} would be adjusted continuously so that the pixel output would reach the potential set by V_{REF}. By choosing a column feedback amplifier with a large gain, one could obtain a large feedback factor during soft reset, with consequent suppression of reset noise by a large factor. Thus, reset noise could be reduced to a level much less than $(kTC_S)^{1/2}/q$. Taking advantage of the large reduction in noise, one could increase full-well capacity without incurring a noise penalty.

Because (1) the additional circuitry (beyond that of a conventional APS) needed in each pixel would be only one additional FET and one additional conductor line and (2) the column feedback amplifiers would be located at the ends of the columns rather than in the pixels, incorporation of the column feedback sub-circuits would entail minimal changes in pixel circuitry that would not compromise quantum efficiency or pixel size. Hence, the proposed imager could feature an unprecedented combination of high quantum efficiency, low noise, small pixel size, and large full-well capacity, all contributing to high performance.

This work was done by Bedabrata Pain, Thomas Cunningham, Bruce Hancock, Suresh Seshadri, and Monico Ortiz of Caltech for **NASA's Jet Propulsion Laboratory**. *For further information, access the Technical Support Package (TSP)* ***free on-line at www.nasatech.com***.

In accordance with Public Law 96-517, the contractor has elected to retain title to this invention. Inquiries concerning rights for its commercial use should be addressed to

Intellectual Property group
JPL
Mail Stop 202-233
4800 Oak Grove Drive
Pasadena, CA 91109
(818) 354-2240

Refer to NPO-21111, volume and number of this NASA Tech Briefs *issue, and the page number.*

BLANK PAGE

Electronic Systems

Hardware, Techniques, and Processes

13 Digital Flash X-Ray Imager for Quantitative Physiology
14 High-Frame-Rate CCD Camera Having Subwindow Capability
14 Stereoscopic Vision System Tracks Objects in Real Time
15 Interface System for Downlinking Digital TV Signals From Spacecraft
15 High-Efficiency Ultraviolet CCD Video Camera for Biology

BLANK PAGE

Digital Flash X-Ray Imager for Quantitative Physiology

Images are corrected for scatter, and dual-energy imaging facilitates discrimination between soft tissue and bone.

Lyndon B. Johnson Space Center, Houston, Texas

An optoelectronic digital flash x-ray imaging system has been invented for use in quantitative physiological studies and general radiology. The system could be implemented in a relatively compact, lightweight apparatus suitable for use aboard a spacecraft as well as on Earth. Applications for which this system is especially well suited include monitoring changes in bone density; monitoring redistribution of fat, muscle, and body fluids; mammography; and three-dimensional tomography.

The system is based on use of imaging devices in the form of the most recently developed large-format planar arrays of integrated semiconductor x-ray detectors. Three especially notable features of the system are the following:

- The system hardware and software are designed so that in digital processing of image data, the contribution of scattering of x-rays is subtracted out, leaving an essentially scatter-free image. This is a significant advantage because scattering tends to reduce contrast, reduce the signal-to-noise ratio, and cause blurring.
- The system employs a dual-x-ray-energy imaging method that facilitates discrimination between soft tissue and bone.
- A compact flash x-ray source makes it possible to obtain stop-motion images.

The design and principle of operation of the system are amenable to several variations. The figure depicts the x-ray imaging geometry of the system to assist in understanding the principle of operation of a basic version of the system. X rays from a compact flash source (regarded as a point source) pass through the human body or other object under examination to an imaging apparatus that comprises an x-ray collimator sandwiched between front and rear x-ray detector assemblies. In this version, the source is capable of generating photons with energies that are concentrated toward either the lower or the higher end of a range from about 10 to about 500 keV, and is operated in such a manner that it alternates between the low and high photon energies on successive pulses.

The x rays that impinge on the front detector assembly include the primary x rays, which are the desired x rays that pass directly from the source to the detectors along radial lines and form the projection image of the body under examination. Scattered x rays (which deviate from the radial lines) also impinge on the front detector assembly. Because all the front detectors are illuminated by both primary and scattered x rays, the front detector assembly yields a high-resolution image.

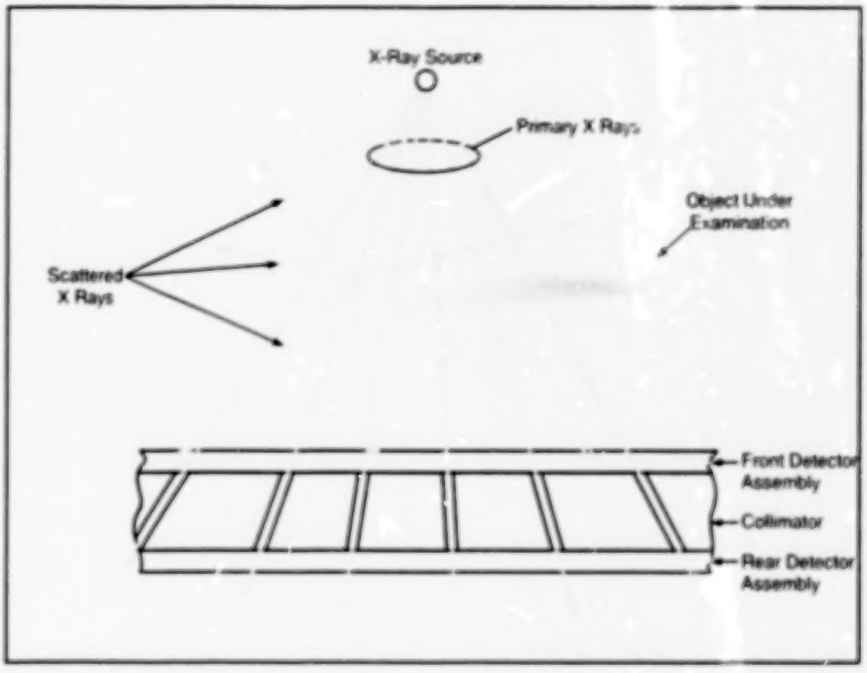

Front and Rear Detector Assemblies and a Collimator aligned with the x-ray source yield image data that make it possible to correct for scattering.

The collimator is made from a plate of an x-ray-absorbing material. Holes that are radial to the x-ray source are drilled or otherwise formed in the plate. These holes are wide enough to pass a detectable fraction of the primary (radially propagating) x rays and not so wide as to pass a substantial fraction of scattered (non-radially-propagating) x rays. Of course, the x rays are blocked from those rear detectors that are covered by the solid portions of the collimator; hence, the image detected by the rear detector assembly is a low-resolution image formed in primary x rays.

To obtain a complete snapshot of the object under examination, one acquires two sets of images: one in low-energy and one in high-energy x rays. The detector outputs are digitized, then processed in a computer to correct for scattering and to determine the amounts of bone and soft tissue along the radial line to each pixel. The processing involves taking account of the differences between the behaviors of the low- and high-energy x rays, the different resolutions of the front- and rear-detector images, and the known radial-line geometric relationships between coordinates in images on the front and rear detector planes. The steps of the image-processing algorithm (somewhat oversimplified to fit the space available for this article) are summarized as follows:

1. The low- and high-energy front- and rear-detector outputs are normalized and corrected for "dark" signals according to established x-ray-image-processing procedures.
2. The quantities of soft tissue and bone along the projection line from the source to each pixel in the low-resolution image are computed from the low- and high-energy rear-detector outputs, by use of a numerical inversion of the equations for attenuation of the low- and high-energy x rays in soft tissue and bone.
3. For each image and each front-detector position connected with a rear-detector position along the projection line of a radial collimator hole, the scatter component of the image is obtained by subtracting front-detector (scatter + primary) reading from the rear-detector (primary only) reading. This operation effectively yields the scatter component of the image.
4. The low-resolution scatter image is interpolated to all pixels between the projection-line points to synthesize a high-resolution scatter image. The interpolation is justified by theoretical calculations and empirical data that show

that scatter has a smooth distribution on an image plane and, consequently, the interpolation error can be assumed to be small.

5. The synthetic high-resolution scatter image is subtracted from the high-resolution front-detector (primary + scatter) image to obtain the desired high-resolution image in primary x rays.

This work was done by Yong-Sheng Chao of Advanced Optical Technologies, Inc., for **Johnson Space Center**.

In accordance with Public Law 96-517, the contractor has elected to retain title to this invention. Inquiries concerning rights for its commercial use should be addressed to

Advanced Optical Technologies, Inc.
111 Founders Plaza
Suite 809
East Hartford, CT 06108

Refer to MSC-23071, volume and number of this NASA Tech Briefs *issue, and the page number.*

High-Frame-Rate CCD Camera Having Subwindow Capability

A 6-kHz frame rate is projected for 8 × 8-pixel subwindows.

NASA's Jet Propulsion Laboratory, Pasadena, California

A custom high-speed charge-coupled-device (CCD) camera that features a capability for real-time readout from multiple regions of interest (subwindows) within its field of view is undergoing development. The camera was designed initially as a means of tracking a remote laser beacon in a free-space optical communication system. The basic camera design is also adaptable to eye-tracking, target-tracking, and machine-vision systems.

The figure depicts the camera as installed in a laboratory test bed. The camera includes a 658 × 496-pixel commercial CCD integrated-circuit chip capable of subwindow readout. The CCD chip is mounted on a circuit card denoted the CCD imager card. Also mounted on the imager card are (1) level-translator and buffer circuitry for the CCD strobe lines and (2) a pair of commercial analog signal-processor chips, each of which performs correlated double sampling, includes a 10-bit analog-to-digital converter, and accommodates serial programming for setting amplifier gain, pixel bias level, and other operational parameters.

A digital signal processor (DSP), mounted on another card, is used to issue commands to, and read images from, the camera. Still another circuit card, denoted the focal-plane-array (FPA) interface card, contains a pair of field-programmable gate arrays that serve as part of an interface between the circuitry on the CCD imager card and the DSP. The rest of the CCD-imager/DSP interface comprises a global bus and custom bus interface logic circuitry, which implements the logic for an address decoder, a handshake mechanism, and data-path buffers for access to the camera via the global bus port of the DSP.

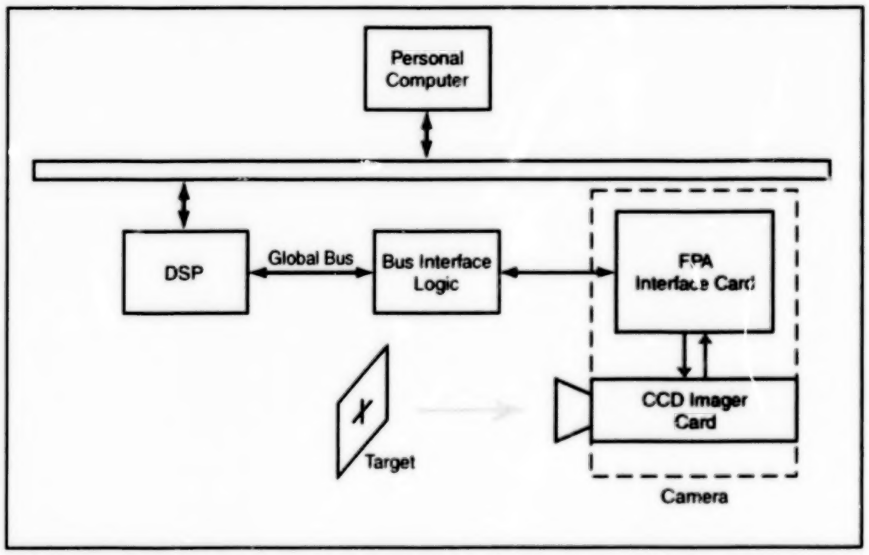

This Block Diagram shows the camera as installed in a test bed built previously for demonstrating acquisition and tracking of a laser beacon for a free-space optical communication system.

Preliminary test data suggests that it is possible to achieve a frame rate of 6 kHz for 8 × 8-pixel subwindows with a pixel resolution and dynamic range of 7 bits. Planned refinements in camera and test bed are expected to increase the frame rate in the fastest area of the CCD to 17 kHz and the pixel resolution to 10 bits.

This work was done by Steve Monacos and Angel Portillo of Caltech for **NASA's Jet Propulsion Laboratory**. *For further information, access the Technical Support Package (TSP)* ***free on-line at www.nasatech.com***.

NPO-30564

Stereoscopic Vision System Tracks Objects in Real Time

A stereoscopic machine-vision system offers a capability for robust tracking of objects in three dimensions (3D). The system is suitable for use in a variety of robotic applications. The system hardware includes a pan-tilt-verge camera-and-aiming-mechanism assembly and a board that holds control and image-data-processing circuitry. Included on the circuit board are circuitry and firmware that perform correlations at the speeds necessary for tracking complex objects in real time. The system software implements algorithms for correlation-based tracking of objects, using stereoscopy. A significant portion of development effort was directed toward solving the problem of gaze control — that is, where to focus attention and vision image-data-processing resources. The chosen solution lies in the stereo-cluster approach, which embodies tenets of active vision. In somewhat oversimplified terms, a stereo cluster can be characterized as a cluster of points, selected on the basis of texture extracted from image data, that appear to bound an object to be tracked and upon which, therefore, attention must be focused. In laboratory tests, the

stereo-cluster approach was demonstrated to enable robust tracking of objects in 3D.

This work was done by Eric Huber and Bryn Wolfe of Metrica, Inc., and Jeff Kerr of JRKerr for **Johnson Space Center**. *For further information, access the Technical Support Package (TSP)* ***free on-line at www.nasatech.com***.

MSC-23113

Interface System for Downlinking Digital TV Signals From Spacecraft

A system of interface electronic circuitry that includes a data packetizer and a data depacketizer has been developed to enable the downlinking of both standard- and high-definition television (SDTV and HDTV) signals from a space shuttle or the International Space Station. The packetizer accepts electronic input of a stream of data from a commercial-off-the-shelf SDTV or HDTV compression encoder that operates according to the MPEG-2 (Moving Pictures Experts Group) standard and outputs the DVB ASI (Digital Video Broadcast Asynchronous Serial Interface) format. The packetizer converts the input stream to an output stream of data packets that conforms to a standard of the Consultative Committee for Space Data Systems (CCSDS) and is compatible with either the Space Station High Rate Frame Map (HRFM) or the space shuttle downlink data multiplexer. The packetizer output circuitry includes a transparent asynchronous transceiver interface (TAXI), which transmits the packets to the downlink data multiplexer or HRFM via a fiber-optic link. The depacketizer is implemented as a printed-circuit board that is plugged into a ground system computer. The ground system displays health and status of the flight system as well as providing the recovered MPEG-2 video for ground use.

This work was done by S. Douglas Holland of **Johnson Space Center**. *For further information, access the Technical Support Package (TSP)* ***free on-line at www.nasatech.com***.

MSC-23304

High-Efficiency Ultraviolet CCD Video Camera for Biology

The frame rate would be variable from 1 to 30 Hz.

NASA 's Jet Propulsion Laboratory, Pasadena, California

A high-efficiency, high-frame-rate ultraviolet (UV) charge-coupled device (CCD) camera that is especially well suited for biological and defense applications was developed. This is the first high-frame rate camera using delta-doped CCDs, which is suitable for biological imaging having high speed, high and stable UV quantum efficiency and insensitivity to visible light.

The camera is built around a back-surface illuminated, thinned, delta-doped CCD with antireflection coating and a visible-light-blocking filter. [Issues pertaining to the principle of operation, design, and fabrication of delta-doped CCDs have been discussed in a number of prior *NASA Tech Briefs* articles, the one most relevant to the present development being "Back-Illuminated CCDs With Integral Ultraviolet-Pass Filters" (NPO-21007), *NASA Tech Briefs*, Vol. 25, No. 7 (July 2001), page 20a.] Back-illuminated delta-doped CCDs have been found to operate at quantum efficiency of 40 to 60 percent in the 300- to 400-nm region of interest. With addition of antireflection coatings, quantum efficiency can be increased to between 80 to 100 percent. Moreover, the high quantum efficiency of delta-doped CCDs has been shown to be stable for years. Because CCDs are also sensitive to visible light, filters must be included to block the light at wavelengths greater than 400 nm.

The camera has been demonstrated to operate at a rate of 2 to 10 frames per second with digital output and digital control of

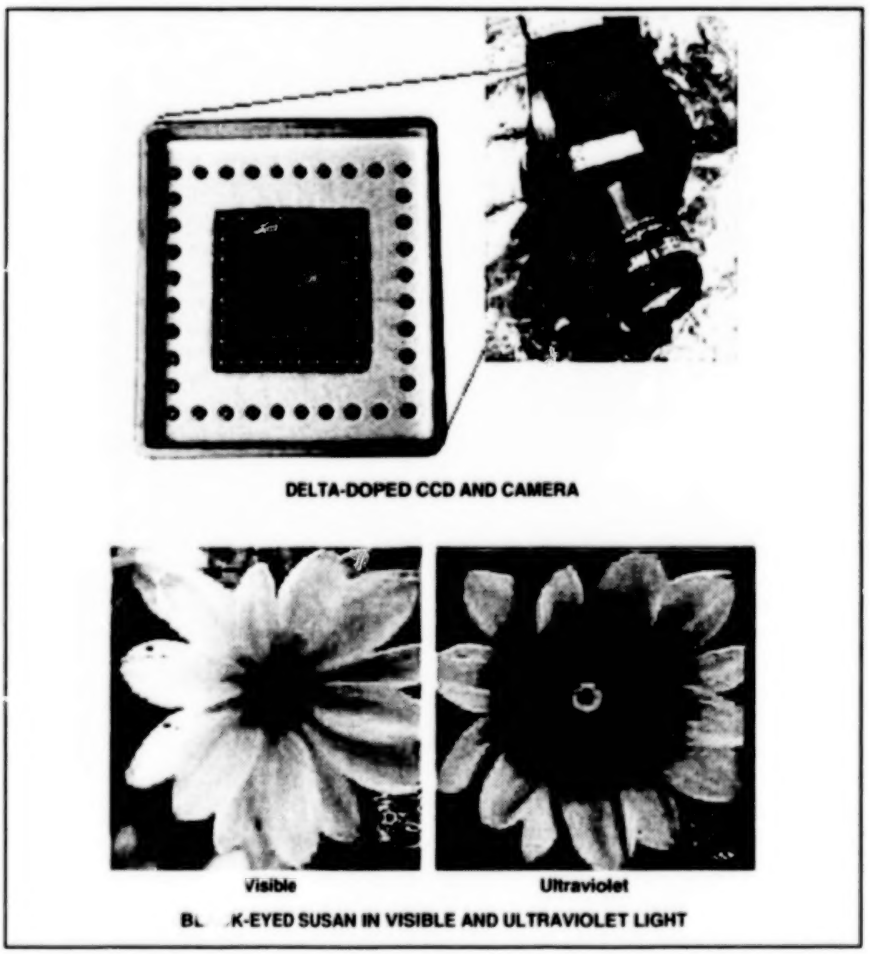

DELTA-DOPED CCD AND CAMERA

BLACK-EYED SUSAN IN VISIBLE AND ULTRAVIOLET LIGHT

The Prototype Camera Was Used To Image a Flower in visible light and then in ultraviolet light with a visible-light-blocking filter. The flower (a black-eyed susan) is among those that have a distinct "bull's eye" appearance in ultraviolet light that helps bees and butterflies recognize it from a distance.

the camera parameters and in acquiring images of biological significance in a wavelength band centered at 300 nm (see figure). At the time of reporting, the camera is operating a delta-doped, 1024-by-1024-pixel, 12-μm-pixel-pitch CCD. Camera electronics are capable of operating at a rate of 30 frames per second and subsequent development is required for design and fabrication of video-rate CCDs for use in this camera. The camera is also compact and transportable and is suitable for field observations as well as laboratory measurements.

This work was done by Shouleh Nikzad and Todd J. Jones of Caltech for **NASA's Jet Propulsion Laboratory**. *For further information, access the Technical Support Package (TSP)* ***free on-line at www.nasatech.com***.

In accordance with Public Law 96-517, the contractor has elected to retain title to this invention. Inquiries concerning rights for its commercial use should be addressed to

Intellectual Assets Office
JPL
Mail Stop 202-233
4800 Oak Grove Drive
Pasadena, CA 91109
(818) 354-2240
E-mail: ipgroup@jpl.nasa.gov

Refer to NPO-30514, volume and number of this NASA Tech Briefs *issue, and the page number.*

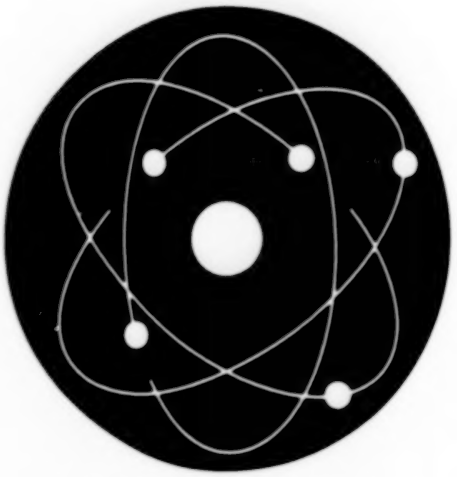

Physical Sciences

Hardware, Techniques, and Processes

19 Compact System Detects Potentially Explosive Gas Mixtures
20 Scanning Thermography
20 Ultrahigh-Vacuum Arc-Jet Source of Nitrogen for Epitaxy

Books and Reports

21 Lightweight Mirrors for Orbiting Earth-Observing Instruments

BLANK PAGE

Compact System Detects Potentially Explosive Gas Mixtures

This system can be used in environments too severe for conventional leak detectors.

Marshall Space Flight Center, Alabama

The figure depicts selected aspects of a "smart," microelectronic-based hazardous-gas-detection system that simultaneously measures concentrations of hydrogen and oxygen. Unlike conventional gas-leak-detection systems built around mass spectrometers, this system is not restricted to operation in relatively mild and controlled laboratory or shop environments; instead, this system can operate over a range of temperatures and pressures. Also, in comparison with conventional mass-spectrometer-based leak-detection systems, this system is more robust and compact, weighs less, and consumes less power.

The design of this system integrates advanced microelectronic hydrogen and oxygen sensors with microelectronic control, data-processing, and communication circuitry. The system includes multiple sensor modules for measuring concentrations of gases at multiple locations simultaneously. Within each sensor module, the gas sensors are mounted together on a small electronic circuit board. A microcontroller, signal-conditioning circuits, a power-supply circuit, a temperature sensor, and a pressure sensor are also contained within each module. The sensors are thin-film, micromachined silicon devices. Firmware in the microcontroller controls the operation of the gas sensors, collects data from the pressure and temperature sensors, performs real-time compensation for pressure effects and thermal drift, converts sensor readings to engineering units, and effects digital communication between the module and external instrumentation. The use of a digital communication interface minimizes the amount of wiring needed for communication.

Although this system was conceived as a prototype of onboard systems for detecting potentially explosive hydrogen/oxygen mixtures aboard reusable launch spacecraft, variants of this system could readily be designed for terrestrial applications (e.g., in hydrogen-fueled vehicles and hydrogen-consuming industrial facilities) in which compact and relatively inexpensive gas-leak detectors are needed. Moreover, sensor modules could be constructed to accommodate interchangeable sensors for measuring gases other than hydrogen and oxygen.

This work was done by Darby B. Makel of Makel Engineering, Inc., for **Marshall Space Flight Center**. *For further information, access the Technical Support Package (TSP)* ***free on-line at www.nasatech.com***.
MFS-31577

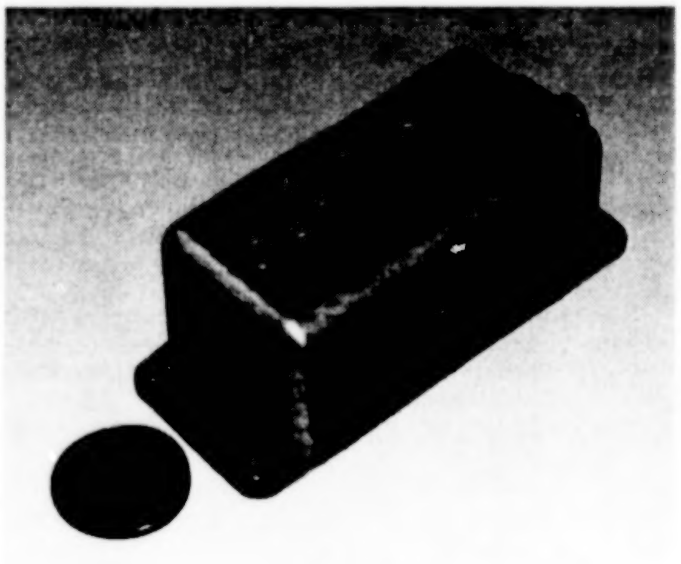

SENSOR MODULE

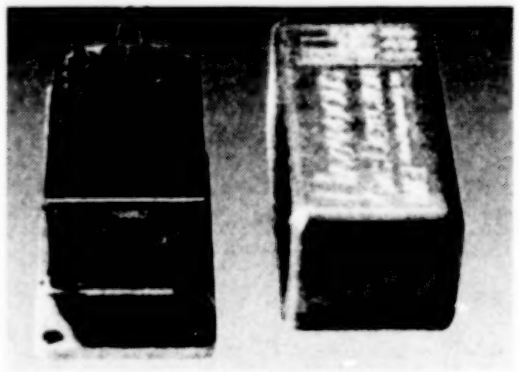

MODULE WITH COVER REMOVED FROM SENSOR CIRCUITRY

SENSOR NETWORK WITH POWER-CONVERTER HUB IN FOREGROUND

Compact Sensor Modules measure concentrations of hydrogen and oxygen simultaneously at multiple locations.

Scanning Thermography

Large objects can be scanned fairly quickly.

Langley Research Center, Hampton, Virginia

Scanning thermography is a noncontact, nondestructive technique that makes it possible to find defects hidden inside structural components in a variety of settings. Scanning thermography can be used to perform inspections of objects that may have large areas and a variety of shapes and that are found in a variety of settings that include, but are not limited to, production lines, industrial tanks and pipes, aircraft, power plants, and bridges. Scanning thermography is applicable to diverse structural materials, including metals, plastics, laminated polymer-matrix composites, and bonded aluminum composites, to name a few. Defects that can be detected by scanning thermography include cracks, disbonds (delaminations), corrosion, and wear.

In scanning thermography, both a source of infrared radiation and an infrared camera are mounted together near an object to be inspected and are kept at constant distance from the object while they are moved together along the surface of the object. The infrared camera images the temperature of the region behind the moving source. The output of the infrared camera is digitized and sent to an image-data processor, which computes spatial variations of temperature across the imaged portion of the surface area. Spatial variations of temperature indicate spatial variations of heat capacities. Because portions of the object that contain damage, corrosion, or delaminations are thinner, and therefore have a reduced thermal mass, relative to portions that do not contain such defects, they exhibit corresponding differences in temperature. The resulting temperature map can be examined and/or the digital output of the image-data processor can be processed further to diagnose the structural degradation.

A scanning thermographic apparatus (see figure) is highly portable. It can scan the surface of an object to be inspected at a rate about six times that of a conventional thermographic apparatus. More specifically, it can scan at a speed that can be varied up a maximum of >6 ft/s (>1.8 m/s). This is fast enough that power-plant boilers, for example, are now being inspected by scanning thermography in a fraction of the time needed for inspection by prior techniques.

Improvements in efficient utilization of the thermal source have increased the signal-to-noise ratio, significantly improving the quality of the postprocessed image data. Compilation of the image data provides a comprehensive archive — an inspection record that can be reviewed over time to provide a means of monitoring the evolution of damage within a particular structure.

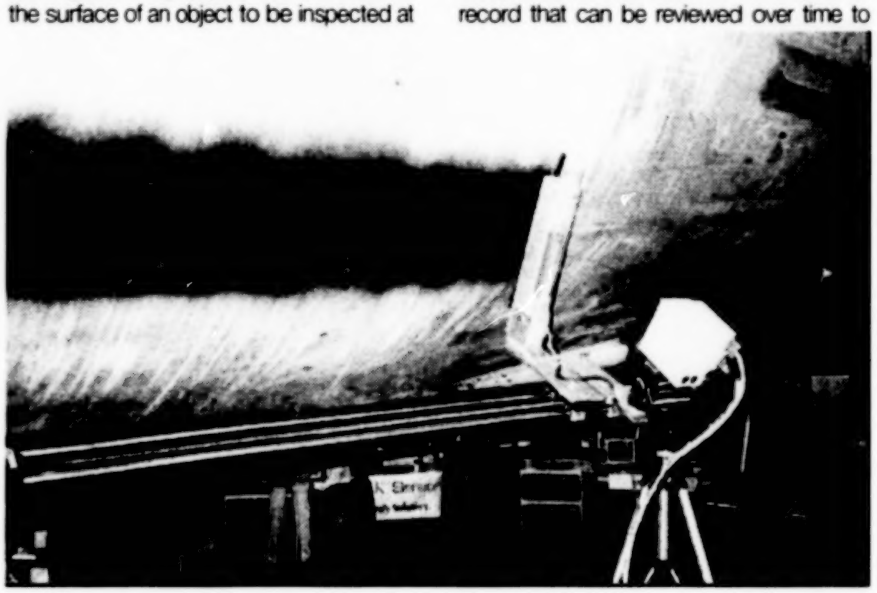

A Scanning Thermographic Apparatus is used to search for defects in the fuselage of a passenger airplane.

This work was done by K. Elliott Cramer and William P. Winfree of **Langley Research Center**. *For further information, access the Technical Support Package (TSP)* ***free on-line at www.nasatech.com***. *LAR-15524*

Ultrahigh-Vacuum Arc-Jet Source of Nitrogen for Epitaxy

Electron-excitation and translational energies can be selected.

NASA's Jet Propulsion Laboratory, Pasadena, California

An arc-jet source of chemically active nitrogen atoms has been developed for use in molecular-beam epitaxy (MBE) to grow such III-V semiconductors as nitrides of gallium, aluminum, and indium. This apparatus utilizes a confined arc to thermally excite N_2 and to dissociate N_2 into N atoms. This apparatus is compatible with other, ultrahigh-vacuum MBE equipment commonly used in growing such materials.

The key technical challenge in the MBE of nitrides of metals in group III in the periodic table is to devise a source of incorporatable nitrogen. Unlike in the growth of the other III-V compound semiconductors by MBE, direct reaction of N_2 with excess group-III metal is not feasible because of the strength of the bond between the N atoms in N_2. To generate incorporatable nitrogen, it is necessary to excite N_2, forming a beam of N atoms, active nitrogen molecules (N_2^*), or N ions. Previously developed radio-frequency- and electron-cyclotron-resonance-based sources utilize electron-impact excitation to obtain monatomic nitrogen and, in so doing, also generate a variety of excited ions and neutrals. Experiments have shown that the ions in the beam from such a source degrade the microstructure of the epitaxial layer and generate electrically active defects. Recent theoretical studies have predicted that ground-state monatomic nitrogen could be incorporated into growing GaN, while monatomic nitrogen in either of its excited doublet states would lead to etching.

Addressing these issues, the present apparatus is designed to generate a beam characterized by a relatively high flux of monatomic nitrogen with selectable electronic and translational energies.

The apparatus (see figure) includes a

constricted nozzle that forms a free jet of a source gas. (In initial experiments to test the apparatus, the source gas was N_2 seeded with 10 percent of Ar to facilitate spectroscopic analysis.) A cathode used to strike an arc passes through the nozzle and a set of skimmer stages that are used to differentially pump the gas delivered by the nozzle. The differential pumping minimizes the pressure in the MBE vacuum chamber. In the arc-jet heater, a high-speed laminar flow of gas forms between a high-pressure zone in the vicinity of the cathode and a low-pressure outlet to the vacuum chamber.

When the arc is ignited, an electron column passing through the nozzle is confined to the very center of the channel by the laminar flow. At the outlet of the nozzle, the pressure changes abruptly, and the electron arc expands radially, attaching to the grounded outer surface of the nozzle, forming an arc foot. The flowing gas is radiatively and convectively heated by the arc plasma during its transit through the nozzle.

The side walls of the nozzle are insulated from convective heating by the boundary layer formed between the nozzle and the high-velocity gas. Depending on the current sustaining the arc and the duration of contact of the gas with the arc plasma, the gas within the nozzle can be heated to temperatures in excess of 7,500 °C. The flowing gas is exposed to possible electron-impact excitation in the region of the cathode and the arc foot as it passes through the arc; however, the duration of this excitation is quite short, so that the generation of ionic species is minimal.

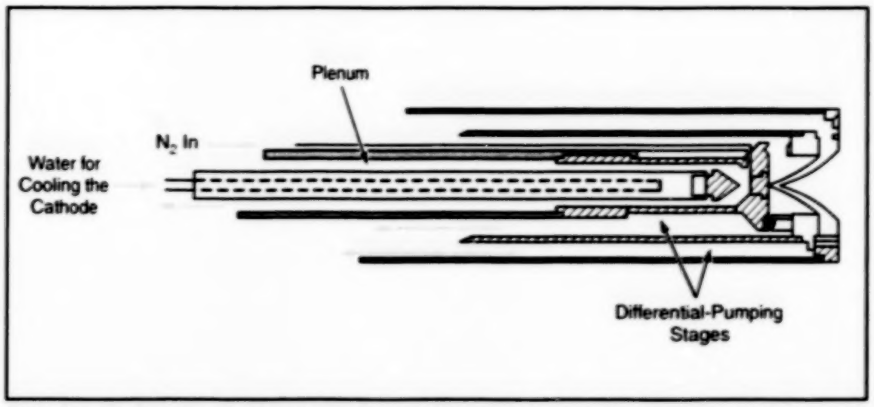

This Arc-Jet Source of Chemically Active Nitrogen incorporates features of both arc-jet thrusters and molecular-beam sources.

The materials, constrictor and nozzle geometry, pressure, and power levels are chosen to minimize the ion yield and maximize the flux of monatomic nitrogen. The cathode is replaceable and cooled by water, and its active part is made of thoriated tungsten. The nozzle is also replaceable and is made of rhenium. The interior plenum near the cathode is made of rhenium. The supporting chamber that contains the nozzle is made of tantalum; the structure that supports the skimmer stages, of molybdenum; and the skimmers, of rhodium. The apparatus is connected with the vacuum chamber through a bellows/manipulator and a gate valve to provide for maintenance and precise alignment to the sample.

The apparatus has been found to be stable and robust and to operate reproducibly from day to day. It has been operated successfully at the lowest power levels (10 to 300 W) reported for an arc jet. Initial experiments have shown that the current density of positive ions in the beam formed by this apparatus is relatively low. It has also been shown that through variation of the parameters of the nitrogen flow and the arc current, one can vary the relative amounts of N_2^+ and monatomic nitrogen. With control of the translational energies and electronic-excitation levels of these active nitrogen species, it should be possible to systematically study the fundamentals of heteroepitaxy of group-III nitrides.

This work was done by Frank Grunthaner and Paula Grunthaner of Caltech; C. Bryson of Surface/Interface, Inc.; and R. Laferla of Ultramet, Inc., for **NASA's Jet Propulsion Laboratory**. *For further information, access the Technical Support Package (TSP)* ***free on-line at www.nasatech.com***.
NPO-20899

Books and Reports

Lightweight Mirrors for Orbiting Earth-Observing Instruments

A report discusses selected aspects of a continuing program to develop thermally stable, lightweight mirrors for planned Earth-observing spaceborne instruments. These mirrors are required to retain precise concave or convex surface figures required for diffraction-limited optical performance, even in the presence of transient, asymmetric thermal loads, which include solar heating and radiational cooling. In the first phase of the program, preliminary analyses were performed to select one of three types of mirror structures: one made of SiC, one made of Be, and a hybrid comprising a lightweight composite-material substructure supporting a glass face sheet that would be a substrate for the required precise optical surface. The hybrid structure was selected for further development because it would offer a combination of high stiffness and low mass and because, relative to the Be and SiC structures, (1) the coefficients of thermal expansion of its constituent materials and the resulting wavefront error would be smaller, and (2) it could be fabricated at lower cost. A prototype hybrid structure with an aperture diameter of 0.3 m was fabricated. Planned efforts in the next phase of the program include optical polishing of the glass face sheet and testing.

This work was done by Greg Mehle and Dan Federico of Composite Optics, Inc., for **Marshall Space Flight Center**. *To obtain a copy of the report, "Thermally Stable Lightweight Mirrors for Earth Observing Instruments," access the Technical Support Package (TSP)* ***free on-line at www.nasatech.com***.
MFS-31799

BLANK PAGE

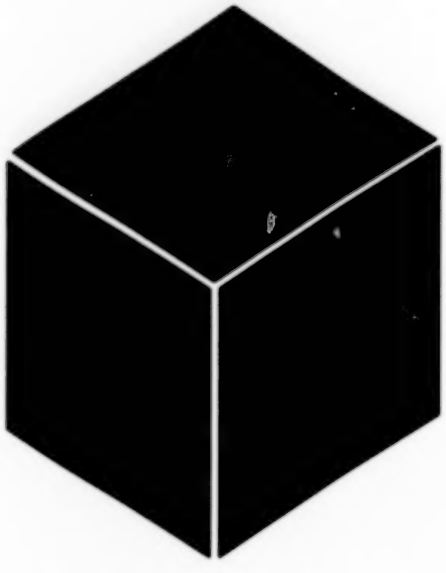

Materials

Hardware, Techniques, and Processes

25 Polymer Electrolytes for Rechargeable Lithium Batteries

BLANK PAGE

Polymer Electrolytes for Rechargeable Lithium Batteries

Cyanoresins would be blended and complexed with Li salts.

NASA's Jet Propulsion Laboratory, Pasadena, California

Polymeric electrolytes for rechargeable lithium-based electrochemical cells and batteries would be made by blending and complexing cyanoresins with lithium salts, according to a proposal. In particular, polymeric electrolytes for separators, carbon-composite anodes, and cathodes would be formulated from appropriate blends of different polymers that are mutually insoluble and do not chemically react with each other. As a result, each polymeric component would retain its specific desired characteristics in high-energy-density batteries that would be capable of long cycle lives and high charge/discharge rates. For example, one polymeric component could provide high ionic conductivity and charge-carrier concentration while another polymeric component would provide structural integrity. Conceivably, a lithium battery made with such materials could exhibit an energy density of 80 W-h/lb for more than 1,000 charge/discharge cycles. Batteries like this could be used in applications ranging from geosynchronous satellites to electric vehicles to small consumer electronic equipment.

Heretofore, lithium anodes normally have not been stable in polymeric-electrolyte batteries because most polymeric electrolytes now in use react unfavorably with freshly plated Li. These interactions may increase the electrical resistances of anode/electrolyte interfaces and, thus, the electrical resistances of the affected cells to unacceptable levels during charge/discharge cycling, and may reduce charge/discharge capacities.

Lithium-ion conductivities in currently available candidate solid polymeric electrolyte materials range between 10^{-6} and 10^{-5} S/cm; these values are too low for effective operation at room temperature. The polymers that have been used to synthesize polymeric electrolytes include polyacrylonitrile, polyvinyl pyrrolidone, and polyethylene oxide, all of which have low dielectric constants (between 4 and 5). Low dielectric constants lead to high degrees of ion association in polymeric electrolytes; this, in turn, results in unacceptably low concentrations of charge carriers and low ionic conductivities at room temperature.

To increase ionic conductivities by the two orders of magnitude as needed for practical cells, the base polymers must be amorphous (with respect to crystalline structure), have low glass-transition temperatures (T_g's), and have large dielectric constants (preferably as large as 20). To prevent failure of cells by maintaining structural integrity of separators (preventing punch-through by lithium dendrites and thereby also preventing electronic conduction between anodes and cathodes), polymeric electrolytes to be incorporated into separators must have T_g's greater than those of polymeric electrolytes to be incorporated into composite-material electrodes. The T_g's of the composite materials in the electrodes must also exceed those of the polymeric electrolytes.

Three commercially available amorphous cyanoresins are under consideration as candidate polymeric electrolytes. These are cyanoethyl polyvinyl alcohol (CRV), cyanoethyl pullulan (CRS), and cyanoethyl sucrose (CRU)(see figure). CRV is a rubbery solid with a relatively low T_g of 30 °C. CRS, which has a T_g of 105 °C and a high molecular weight (760,000) has been studied for use in capacitors and can be processed to form excellent thin films. CRU is a viscous liquid at room temperature, with a molecular weight of 782. These cyanoresins are ideal candidates to be blended and complexed with appropriate Li salts to form polymeric electrolytes of various T_g's for use with composite electrodes and as cell separators with high ionic conductivities. Conventional candidate Li salts include $LiClO_4$, $LiPF_4$, and $LiCF_3SO_3$.

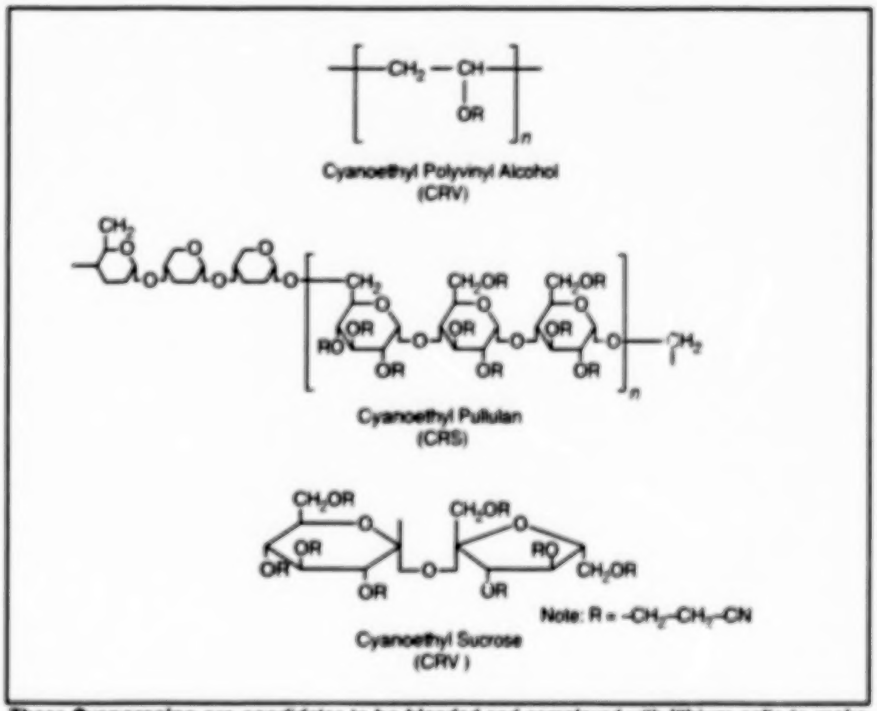

These Cyanoresins are candidates to be blended and complexed with lithium salts to make polymeric electrolytes.

Measurements of the dielectric constants and dielectric-loss characteristics of these three cyanoresins and of CRS/CRV and CRS/CRU blends indicate that the room-temperature dielectric constants are approximately 20 — large enough to achieve high ionic conductivities at nominal temperatures when these cyanoresins complexed with Li ions to form solvent-separated ion pairs. Li salts of CRU and CRV are expected to exhibit restricted anion mobilities, with concomitant high Li^+ mobilities.

This work was done by Shiao-Ping S. Yen, Andre H. Yavrouian, James B. Stephens, and John D. Ingham of Caltech for **NASA's Jet Propulsion Laboratory**. *For further information, access the Technical Support Package (TSP)* ***free on-line at www.nasatech.com***.

NPO-19116

BLANK PAGE

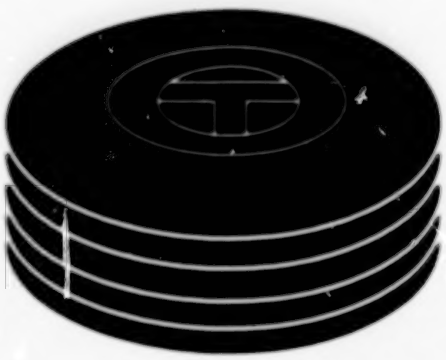

Computer Programs

Materials

29 ICAN/JAVA: Integrated Composite Analyzer Recoded in Java

Mathematics and Information Sciences

29 Software for Monitoring Performance of Other Software
29 Software for Multidisciplinary Analysis With Parallelization
29 Software for Onboard Autonomy of a Three-Spacecraft Mission
30 Software for Mobile Data-Communication Networks
30 Runge-Kutta Circular-Advection-Problem Solver

BLANK PAGE

Materials

ICAN/JAVA: Integrated Composite Analyzer Recoded in Java

The Integrated Composite Analyzer (ICAN) computer program, originally written in the FORTRAN language, has been completely recoded in Java to make it more widely usable. Whereas the original ICAN could be executed on only a limited number of platforms, ICAN/JAVA is compatible with almost all computers and operating systems. Moreover, whereas the original ICAN was applicable to only polymer-based composite materials containing circular fibers, ICAN/JAVA is applicable to diverse composites, including those that contain metal matrices, ceramic matrices, noncircular fibers, and/or particulate reinforcements. ICAN/JAVA can be used to simulate many aspects of the behavior and properties of a composite material and its constituent materials, including vibration-damping and electrical properties. The code includes provisions for three-way substructuring of fiber, interphase, and matrix constituents. Graphical output and telescoping of scale are available. The code includes an on-line user's manual. The Java Runtime Environment software, which can be downloaded free of charge for most platforms, is necessary for execution of ICAN/JAVA.

This program was written by Louis M. Handler and Christos C. Chamis of **Glenn Research Center**. *For further information, access the Technical Support Package (TSP)* ***free on-line at www.nasatech.com***.

Inquiries concerning rights for the commercial use of this invention should be addressed to NASA Glenn Research Center, Commercial Technology Office, Attn: Steve Fedor, Mail Stop 4–8, 21000 Brookpark Road, Cleveland, Ohio 44135. Refer to LEW-17247.

Mathematics and Information Sciences

Software for Monitoring Performance of Other Software

Performance Logging Services (PLS) is a software utility that tracks the performance of another program in terms of statistics of timing and use of memory buffers. The monitored program must utilize either the Unix or the VxWorks operating system. PLS can monitor performance requirements in real time and uses minimal memory and central-processing-unit (CPU) resources. It can measure software timing events with an accuracy of less than 50 μs. PLS consists of (1) a library of application-program interfaces (APIs) and (2) a performance-control-tool subprogram. The APIs are incorporated into a program to be monitored by simply compiling them with the program code. During execution, the APIs update performance statistics in shared memory, to which an external program can gain access. An operator can use the performance-control tool to gain access to the statistics, reset the statistics, and set control limits (essentially, upper and lower limiting values of statistics). The performance-control tool includes a trigger that can be used to start another program when the control limits are exceeded. Data from the triggered program is used to find the source of timing glitches and/or otherwise assist in troubleshooting when performance requirements are out of specification.

This program was written by Terry Ross of **Kennedy Space Center**. *For further information, access the Technical Support Package (TSP)* ***free on-line at www.nasatech.com***.

KSC-12343

Software for Multidisciplinary Analysis With Parallelization

HiMAP is an advanced, portable software system that implements highly modular, parallel computation of the possibly nonlinear, coupled behaviors of aeroelastic and other complex systems that comprise subsystems, each of which is modeled by use of software formulated within a separate technological discipline (e.g., fluid dynamics, structural dynamics, and controls). HiMAP is designed to be executed on massively parallel processors (MPPs) and workstation clusters based on a multiple-instruction, multiple-data architecture. Software for solving the differential equations of the fluids discipline (the Navier-Stokes equations) is parallelized according to a zonal approach; that of the structures discipline is parallelized according to a substructures approach. Computations within each discipline are spread across processors by use of a standard message-passing interface (MPI) for interprocessor communications. Computations that involve exchange of information among disciplines are parallelized by use of MPIAPI — a utility software library that flexibly allocates a group of processors and enables communication between processors within the same group or in different groups. Additional parallelization for multiple-parameter cases is implemented by use of a script software subsystem. The combined effect of the three levels of parallelization is an almost linear scaleability for multiple concurrent analyses performed efficiently on MPPs.

This program was written by Guru Guruswamy, Mark Potsdam, and Neal Chaderjian (NASA Ames Research Center); Chansup Byun (Sun Microsystems); Shigeru Obayashi (Tohoku University, Japan); and Lloyd Eldred (NASA Langley Research Center). Primary development was conducted at **Ames Research Center**. *For further information, access the Technical Support Package (TSP)* ***free on-line at www.nasatech.com***.

ARC-14504

Software for Onboard Autonomy of a Three-Spacecraft Mission

A system of software has been designed to enable autonomous operations of the three University-built miniature spacecraft of the Three Corner Sat mission, scheduled for launch in 2003. The main software subsystems and their functions are the following:

- The Spacecraft Command Language (SCL) robust-execution program will demonstrate aspects of low-level autonomy, including event-driven execution, local retries, low-level responses to faults, and validation of commands.
- The Continuous Activity Scheduling Planning Execution and Replanning (CASPER) program will demonstrate onboard continuous planning to enable the 3CS constellation to respond to mission anomalies, mission opportunities, and onboard evaluations of scientific data, thereby utilizing feedback to integrate planning with execution.
- A data-validation module will use heuristic methods to score utility of scientific images; CASPER will then use the utility scores in planning future operations, discarding images of low-

est utility, and prioritizing downlink resources to send the best images first.

- The Selective Monitoring (SELMON) anomaly-detection-and-isolation program will use empirically derived error bounds to enable context-sensitive detection of anomalies.
- A package of basic spacecraft-coordination software will ensure that one of the spacecraft takes charge of maintaining the plan of operations for all three spacecraft.

This program was written by Barbara Engelhardt, Colette Wilklow, Gregg Rabideau, Robert Sherwood, Russell Knight, and Steve Chien of Caltech for **NASA's Jet Propulsion Laboratory**. *For further information, access the Technical Support Package (TSP)* ***free on-line at www.nasatech.com***.

This software is available for commercial licensing. Please contact Don Hart of the California Institute of Technology at (818) 393-3425. Refer to NPO-30277.

Software for Mobile Data-Communication Networks

Mobile Router is operating system code residing in a network router allowing the router to provide mobile-ipv4 functionality for any attached nodes. Mobile Router enables the entire network to roam. It is no longer necessary for every node in the network to run mobile Internet Protocol (IP) software because Mobile Router provides this function. In addition, Mobile Router eliminates the need to reconfigure a router as it moves from one network to another network, even across network domains. For example, Mobile Router enables communication with aircraft via the Internet and/or intranets. Information as weather data, air-traffic control messages, voice communications, and images could be transmitted to aircraft easily and inexpensively by use of Internet protocols. As another example, data-communication nodes running Mobile Router could be incorporated into ambulances to provide real-time data communications with hospitals and medical experts. Commercial applications could include the provision of mobile Internet connections for cargo and cruise ships, tour buses, passenger aircraft, and automobiles.

This program was written by Kent Lueng and the Cisco Systems mobile networking Internetworking Operating Systems (IOS) team. Daniel Shell of Cisco Systems and William D. Ivancic and the advanced networking research team at **Glenn Research Center** *performed the early field trials and tested, fielded, and provided much needed feedback for the development of features and functions needed for mobile networking. For further information, access the Technical Support Package (TSP)* ***free on-line at www.nasatech.com***.

Inquiries concerning rights for the commercial use of this invention should be addressed to NASA Glenn Research Center, Commercial Technology Office, Attn: Steve Fedor, Mail Stop 4–8, 21000 Brookpark Road, Cleveland, Ohio 44135. Refer to LEW-17322.

Runge-Kutta Circular-Advection-Problem Solver

Release 3.0 of the Multi-Stage Runge-Kutta Circular Advection Solver is a computer program that solves the circular-advection problem by use of a general m-stage Runge-Kutta scheme (for m = 1, 2, and 4) on a Cartesian (x,y) grid with optimized coefficients. [The circular-advection problem, $\partial u/\partial t = (-y,x) \cdot \mathrm{grad}(u)$ is a classical model of convective phenomena suitable for studying the behaviors of algorithms.] The spatial discretization in this software is that of a cell-centered upwind finite-volume formulation. The software is presented as an extensible object-oriented class library arranged so that the components of the Runge-Kutta algorithm can be instantiated arbitrarily from within another computer program. The software includes a complete library wrapper that enables launching of the rest of the software from a command line by use of consistent Unix-style filter conventions. The source code was developed by use of the Extreme Programming (also known, variously, as "eXtreme Programming" and "XP") methodology, and as such is self-revealing, modular, compact, extendable, and customizable. A unique feature of this program is a provision for comprehensive automated testing. All library classes are bundled with complete verification tests, both documenting the feature behavior and enabling extension by end users. Developers have instant feedback from the automated tests if their extensions conflict with the existing code base. Further, a full set of automated validation tests is included to prove various numerical definitions such as positivity or order property of the solver.

This program was written by William A. Wood and William L. Kleb of **Langley Research Center**. *For more information, the authors may be contacted via e-mail at the following:*

W.A.WOOD@LaRC.NASA.gov

The software development, but not the code itself, is described in Wood, W.A., Kleb, W.L., "Extreme Programming in a Research Environment," Springer-Verlag LNCS 2, pp 89-99, August 2002.

LAR-16494

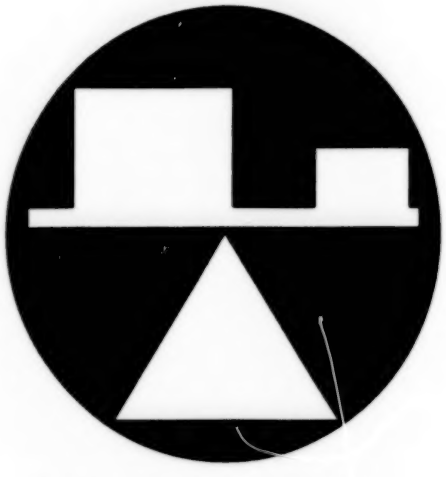

Mechanics

Hardware, Techniques, and Processes

33 Releasable Conical Roller Clutch for Knee Brace

34 Three-Degree-of-Freedom Parallel Mechanical Linkage

BLANK PAGE

Releasable Conical Roller Clutch for Knee Brace

The clutch could also be modified and adapted to other applications.

Marshall Space Flight Center, Alabama

A compact conical roller clutch can be either (1) engaged to obtain both positive locking against rotation in one sense and freewheeling in the opposite sense or (2) disengaged to obtain free rotation in both senses. This clutch was devised to enhance the functionality and increase the durability of the orthotic knee brace described in "Knee Brace Would Lock and Unlock Automatically" (MFS-28991), *NASA Tech Briefs*, Vol. 19, No. 12 (December 1995), page 28. In the knee brace, the clutch can be actuated selectively to prevent undesired flexion when weight is applied or to allow both flexion and extension when weight is not applied or when it is desired to exercise leg muscles.

Previously, the knee brace contained a clutch in which locking was achieved by exploiting friction between padded mating conical surfaces. One disadvantage of that design was that the relatively soft padding deteriorated with repeated actuation. Another disadvantage is that when engaged, the clutch locked against rotation in both senses (preventing both extension and flexion), instead of desirably preventing flexion while allowing extension. The present clutch achieves locking by jamming (wedging) of rollers in tapered pockets, as described in more detail in subsequent paragraphs. The hard roller and pocket surfaces withstand repeated actuation much better than did the soft padding of the previous clutch.

The figure shows the knee-joint mechanism equipped with the present releasable conical roller clutch. The mechanism includes an upper and a lower housing connected via a needle bearing that allows free rotation.

The conical roller clutch includes rollers in tapered pockets in a conical inner surface of the upper housing. A cage retains the rollers in the pockets. Together, the pockets and cage keep the rollers in their nominal positions and orientations in loose contact with a conical surface of the lower housing. The cage and rollers are retained by clips that are attached to the upper housing by screws. Return springs in the cage bias the rollers toward the wide ends of the tapered pockets (the free-rotation position).

A cam in the enclosed space between the upper and lower housings rotates about a pin affixed to the lower housing. The cam includes an elongated lever portion that passes through a slot in an actuation rod and rests against a back plate attached to the upper housing. The actuation rod is mounted in a passage in the lower housing. The movement of the actuation rod is controlled by a cable that

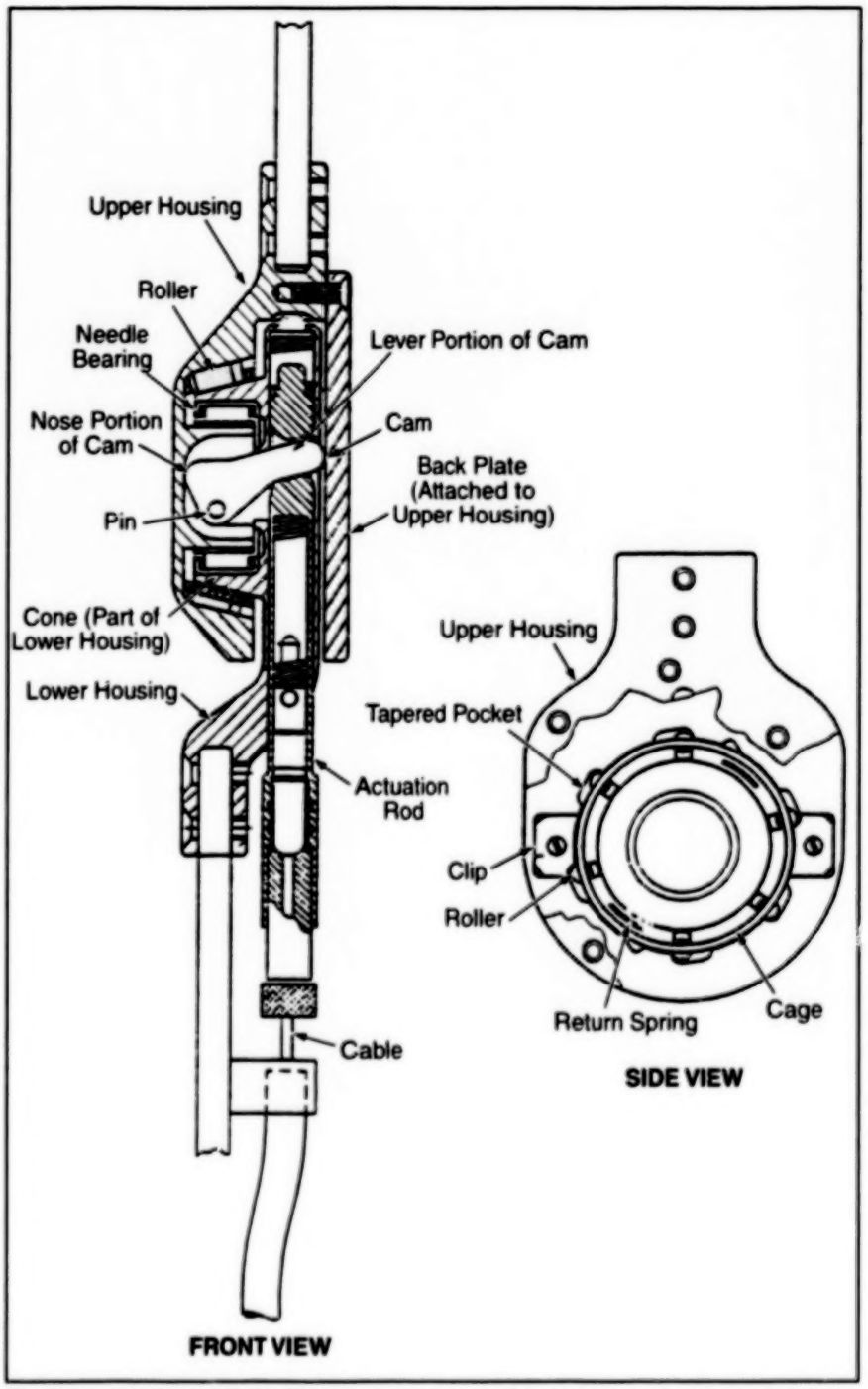

The Releasable Conical Roller Clutch is an integral part of the joint mechanism of an orthotic knee brace. Locking against counterclockwise (in the side view) rotation of the lower housing is achieved by forcing the upper and lower housings together along the axis of rotation to promote wedging of the rollers between the cone and the walls of the tapered pockets. To prevent jamming and thereby provide freedom for both counterclockwise and clockwise rotation, the upper and lower housings are moved slightly apart along the axis of rotation.

can be pulled, for example, by a mechanism sensitive to a load applied to the wearer's foot, described in "Heel-Strike Mechanism for Rehabilitative Knee Brace" (MFS-28992), *NASA Tech Briefs*, Vol. 20, No. 11 (November 1996), page 72.

When the cable is pulled downward, the actuation rod pulls downward on the lever portion of the cam, forcing the back plate and upper housing to the right (as depicted in the front view) and thereby forcing the rollers into contact with both the cone of the lower housing and the walls of the tapered pockets in the upper housing. In this condition, if one attempts to rotate the lower housing counterclockwise relative to the upper housing as depicted in the side view, then the rollers become jammed between the cone and the pocket walls; the resulting wedging force prevents further relative rotation. On the other hand, if one attempts to rotate the lower housing clockwise in the side view, then the rollers are moved toward the wide ends of the tapers; there is no jamming, and consequently rotation can continue freely.

When the cable is not pulled downward, a return spring pushes the actuation rod upward, causing the nose on the left (as depicted in the front view) end of the cam to push the upper housing to the left. This action disengages the rollers from the cone. As a result, there is no opportunity for jamming, and the lower housing can rotate freely, either clockwise or counterclockwise, relative to the upper housing.

The present clutch can be modified and adapted to different applications. For example, if it were to contain equal numbers of tapers in opposite senses of rotation, then the clutch would lock against rotation in both senses during engagement, yet would still allow free rotation in both senses during disengagement.

The present clutch occupies less space than does an equivalent conventional friction clutch. Inasmuch as it can be disengaged to allow free rotation in both senses, the present roller clutch offers an advantage over other roller and sprag clutches that allow free rotation in one sense but always lock against rotation in the opposite sense.

This work was done by Neill Myers of **Marshall Space Flight Center**. *For further information, access the Technical Support Package (TSP)* ***free on-line at www.nasatech.com***. *Refer to MFS-31258.*

Three-Degree-of-Freedom Parallel Mechanical Linkage

Applications could range from microsurgical manipulators to derricks.

Ames Research Center, Moffett Field, California

Figure 1 depicts a mechanical linkage that converts rotational motion about three base joints (A, B, and C) to translational motion of an end effector (D) in three dimensions. The linkage is fully forward- or back-driveable: It can be driven by motors at joints A, B, and C to obtain a desired translation of end effector D, or else it can be driven in translation at end effector D to generate rotations that can be measured (for example, by use of shaft-angle encoders) at joints A, B, and C. Mechanisms based on this one could be particularly useful as compliant robotic manipulators, force-reflecting hand controllers for such manipulators, and manual position-input devices for computers and other systems (see Figure 2).

The linkage is termed "parallel" because of its multiple pathways between end effector and base. In comparison with serial linkages, which have a single pathway between effector and base, parallel linkages typically have greater structural stiffness.

The linkage is composed solely of rigid link members and simple rotary joints arranged in three conjoined kinematic loops. Two of these loops are spherical (i.e., in either loop, all joint axes intersect at a common center point) and include the base joints A, B, and C. The third loop is planar (i.e., all its joint axes are parallel), with one of its links including the end-effector, D. For the configuration illustrated in Figure 1, the intersection of the axes of joints A, B, and C (the origin of the X-Y-Z frame) forms the center of a spherical work volume within which the end effector can move.

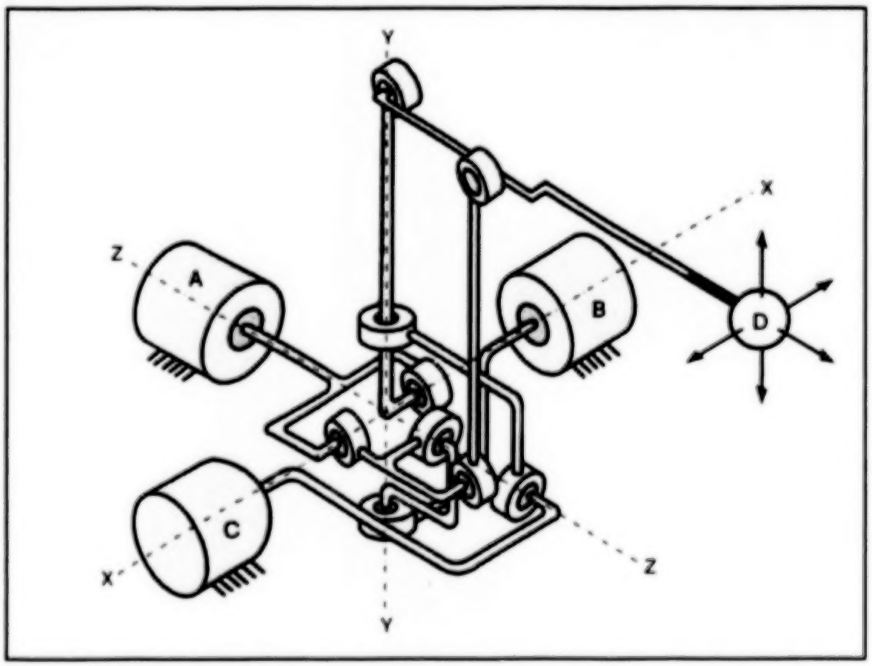

Figure 1. This Schematic Diagram shows the geometry and basic kinematic features of the linkage.

The advantages afforded by this mechanism are the following:

- *Scaleability* — The basic design can be scaled down to devices as small as micromanipulators for advanced surgery or up to machines as large as derricks and cranes.
- *Large Work Volume* — Unlike other parallel linkages, this linkage features very large reachable work space, approaching that of open-loop serial linkages of similar size.
- *High Stiffness* — The inherent stiffness of parallel linkages in general is increased by the use of a minimal number of joints.

Figure 2. A Hand Controller based on the design illustrated in Figure 1 could serve as an input device for a variety of systems that operate under manual control.

The high stiffness, in turn, contributes to accuracy in control of the position of the end effector.

- *Negligible Friction and Backlash* — These advantages result principally from elimination of cables, belts, gears, pulleys, and/or lead screws to transfer motion between rotary motors and the end effector.
- *Low Inertia and Moving Weight* — Requirements for power, force, and structural reinforcement are reduced by eliminating the need to carry large, bulky motors: all motor housings are always fixed to ground.
- *High Force and Power Output* — More (relative to typical other mechanisms of similar size) force and power are available for output because less actuator force must be expended to counteract friction losses and/or to support excessive linkage and actuator weight.
- *Simplified Fabrication and Assembly* — Despite the multiple-loop parallel configuration of this mechanism, there are few alignment prerequisites for successful assembly and operation.

This invention has been patented by NASA (U.S. Patent No. 5,816,105). Inquiries concerning nonexclusive or exclusive license for its commercial development should be addressed to the Patent Counsel, Ames Research Center, (650) 604-5104. Refer to ARC-14066.

BLANK PAGE

Machinery

Hardware, Techniques, and Processes

39 Fail-Safe Electromagnetic Motor Brakes

Books and Reports

40 Optimization of Orientations of Spacecraft Reaction Wheels

BLANK PAGE

Fail-Safe Electromagnetic Motor Brakes

These brakes also offer relatively high energy efficiency.

Lyndon B. Johnson Space Center, Houston, Texas

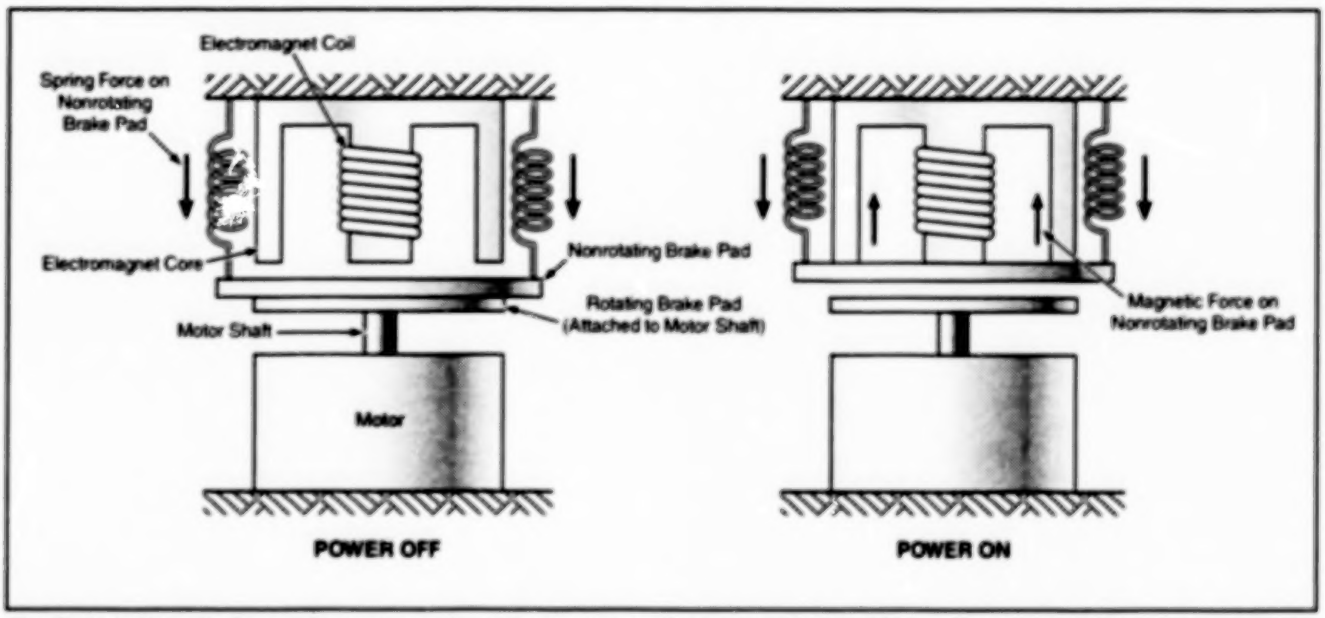

The Brake Is Normally Engaged by spring-loading of the two brake pads against each other. When power is supplied to the electromagnet, the nonrotating brake pad is pulled away from the motor-shaft brake pad.

Fail-safe electromagnetic motor brakes are undergoing development for use in joints of robot arms. The brakes are needed for both static holding and emergency stopping. In the present context, "fail-safe" signifies that a brake disengages (that is, allows motion) when electric power to the brake is turned on and engages (restrains against motion) when the power is turned off. These fail-safe brakes are intended to replace commercial off-the-shelf (COTS) electromagnetic brakes that are large, complex, power-hungry, and hot-running.

A fail-safe brake of this type (see figure) includes a brake pad that is attached to and rotates with a motor shaft, and a nonrotating brake pad in the form of a ferromagnetic plate. An electromagnet collinear with the motor and the brake pads is positioned a short distance from the ferromagnetic plate. When power is not supplied to the electromagnet, a torsionally stiff compression spring pushes the nonrotating brake pad axially into contact with the rotating one. The friction between the two brake pads effects the braking action; in other words, the brake is engaged. When sufficient power is supplied to the electromagnet, the nonrotating brake pad is pulled axially away from the rotating brake pad, thereby disengaging the brake. The spring offers an ancillary benefit in that its small torsional compliance absorbs torsional impulses (caused, for example, by unintended impacts of the robot against external objects), thereby helping to prevent damage to vulnerable motor-drive components.

The basic design concept has been proven in tests on a lifting-electromagnet model. Alternative fail-safe brake designs have been analyzed by use of a mathematical model of the electromagnet. Input design parameters include those of the material, shape, and size of the electromagnet core; the size and the number of turns of the electromagnet wire; and the supply voltage. Outputs of the model include the electromagnet current, power consumption, magnetic-flux density, and force on the ferromagnetic plate.

This analysis has led to a tentative optimum design for a fail-safe brake for a specific application in which the brake is required to hold against a torque of 0.5 lb-ft (≈0.68 N-m). The power required to disengage this brake would lie between 0.025 and 0.040 W. In contrast, the COTS brake that this brake is intended to replace must be supplied with a power of 8 W (at least 200 times as much power) to keep it engaged. Under a typical operational scenario, this comparison translates to much lower time-averaged power consumption for the present design. As an additional benefit stemming from lower power consumption, the fail-safe brake would run cooler than the COTS brake does.

This work was done by James David Jochim of **Johnson Space Center**. *For further information, access the Technical Support Package (TSP)* ***free on-line at www.nasatech.com***.

MSC-23067

Books and Reports

Optimization of Orientations of Spacecraft Reaction Wheels

A report presents a method of optimizing the orientations of three reaction wheels used to regulate the angular momentum of a spacecraft. The method yields an orientation matrix that minimizes mass, torque, and power demand of the reaction wheels while maximizing the allowable duration between successive angular-momentum dumps. Each reaction wheel is parameterized with its own unit vector, and a quadratic cost function is defined based on requirements for torque, storage of angular momentum, and power demand. Because management of angular momentum is a major issue in designing and operating an orbiting spacecraft, an angular-momentum-management strategy is parameterized and included as

part of the overall optimization process. The optimization problem is decomposed by use of a *QR* factorization of the orientation matrix, such that an orthogonal rotation matrix (*Q*) and an upper triangular skewness matrix (*R*) of the wheel frame can be optimized separately. Rotation is optimized analytically (and globally) using a new result for optimizing a Frobenius norm cost over the class of $n \times n$ orthogonal matrices. Skewness is optimized following a sequential-quadratic-programming approach. The report describes several case studies, including one of a spacecraft proposed to be placed in orbit around Europa (the fourth largest moon of Jupiter).

This work was done by David S. Bayard of Caltech for **NASA's Jet Propulsion Laboratory**. *To obtain a copy of the report, "An Optimization Approach to Orienting Three Spacecraft Reaction Wheel Actuators with Application to the Europa Orbiter," access the Technical Support Package (TSP)* ***free on-line at www.nasatech.com***

NPO-30526

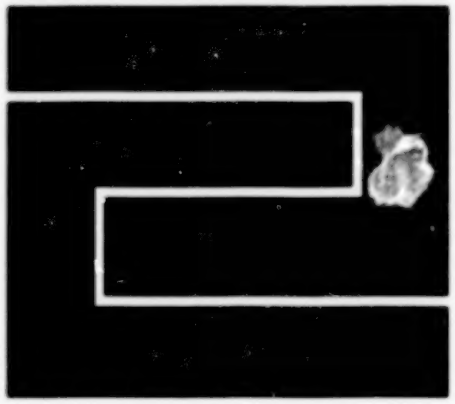

Fabrication Technology

Hardware, Techniques, and Processes

43 Deforming Fibrous Insulating Tiles To Fit Curved Surfaces

44 Micromachining of a Mesoscale Vibratory Gyroscope

42

BLANK PAGE

Deforming Fibrous Insulating Tiles To Fit Curved Surfaces

Flat billets are heated and pressed gently against curved mold surfaces.

Ames Research Center, Moffett Field, California

A curved tile of refractory silica-fiber-based or alumina-fiber-based thermal-insulation material can be formed from an initially flat billet in a process that includes pressing against a curved mold surface during heating. The mold or tile curvature can be concave or convex. Curved tiles are needed for thermal protection of curved surfaces of spacecraft reentering the terrestrial atmosphere; curved thermal-protection tiles may also be useful on Earth in some industrial applications.

The present process was invented as an alternative to the conventional practice of fabricating curved tiles by computer-controlled machining of flat billets, and to facilitate the fabrication of tile areas with dimensions that exceed the customary ≈6 × 6 in. (≈15 × 15 cm). One disadvantage of machining large tiles with curved surfaces is that one must start with relatively thick flat billets and then waste considerable amounts of material. In addition, machining operations become difficult and cumbersome on a large scale, and the computer-controlled milling machines needed to machine large curved surfaces are expensive. Another consequence of machining is that not all the fibers are oriented parallel to the curved surface; this is disadvantageous in that the degree of thermal protection decreases with increasing departure from parallelarity.

The present process makes it possible to manufacture larger curved tiles starting from thinner billets [typical approximate dimensions 10 × 10 ×1/4 in. (≈25 × 25 × 0.6 cm)] with little or no machining of tile material. Unlike in the conventional approach, there is no particular great difficulty associated with fabrication of larger tiles. In addition, the process inherently causes the fibers in a curved tile to lie locally parallel to the curved surface to be protected by the tile.

The figure illustrates an example of the process as applied to forming a tile with a spherical curvature. In this case, a flat billet is placed over the opening in a concave mold. The width of the billet slightly exceeds the diameter of the opening in the mold, so that the billet covers the opening and there is some margin. A weighting ring is placed over the billet, concentrically with the mold. The outer diameter of the ring is slightly less than the diameter of the opening, so that the weight of the ring urges the billet downward into the mold.

The mold is made of a rigid, hard refractory material that can be similar to that of the billet. The weighting-ring material can also be similar to that of the billet and/or the mold. In any event, the mold and weighting-ring materials must be selected so that their coefficients of thermal expansion closely approximate that of the billet.

The assembly of the mold, billet, and weighting ring is placed in a furnace that has been preheated to a temperature of 2,000 °F (≈1,100 °C). Next, the temperature is raised at a steady rate for one hour to a maximum of 2,400 °F (≈1,300 °C), then held at this maximum level for one hour. During the residence at the maximum temperature, the weight of the ring deforms the billet until the lower surface of the billet conforms to the surface of the mold. At the completion of exposure to the maximum temperature, the furnace is cooled steadily for one hour to 2,000 °F (≈1,100 °C), then the assembly is removed from the furnace.

Optionally, before pressing and heating, the outer surface of the billet can be impregnated with a coating material. During the heating, the coating becomes sintered into the billet, forming an outer layer with high surface emissivity.

After the assembly has cooled, a graphite or fiberglass cloth impregnated with an epoxy, polyimide, or other suitable adhesive is placed on the inner surface of the billet and cured in place to form a support structure.

This work was done by Paul Kolodziej, Joe A. Carroll, and Dane Smith of **Ames Research Center**. *For further information, access the Technical Support Package (TSP)* ***free on-line at www.nasatech.com***.

This invention has been patented by NASA (U.S. Patent No. 5,705,012). Inquiries concerning nonexclusive or exclusive license for its commercial development should be addressed to the Patent Counsel, Ames Research Center, (650) 604-5104. Refer to ARC-14051.

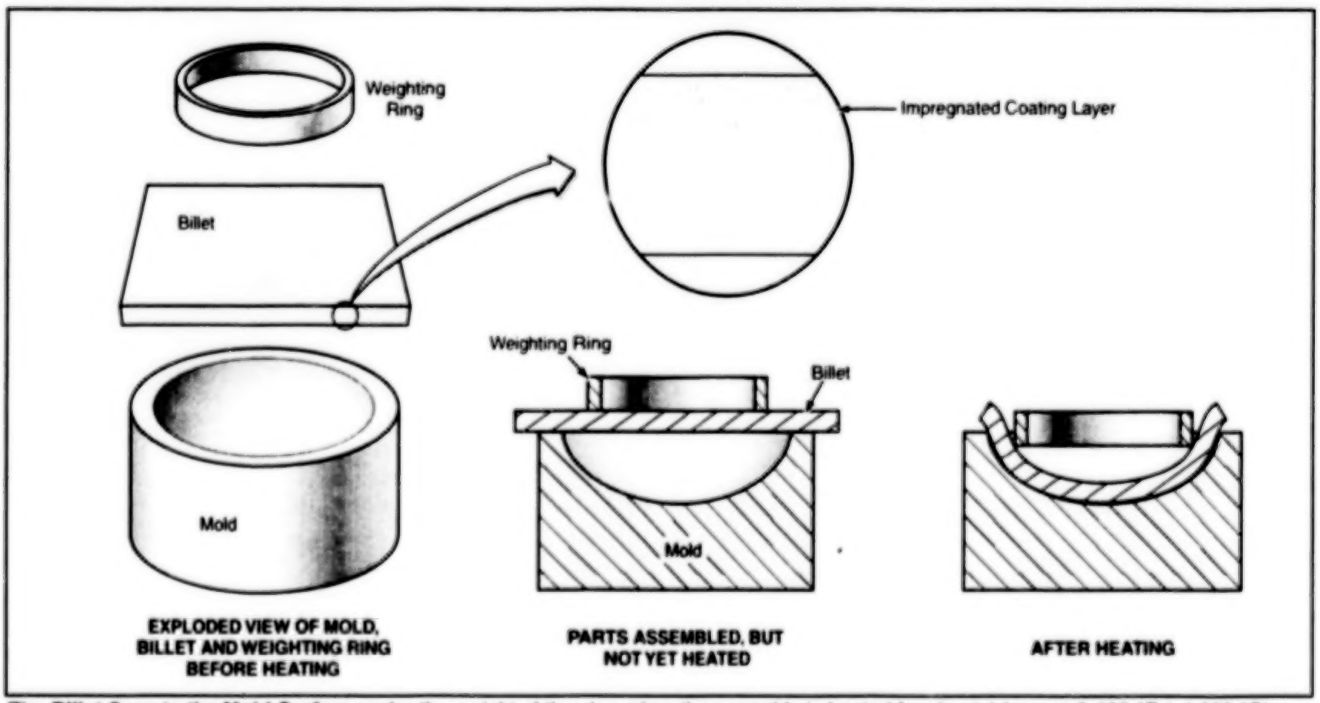

The Billet Sags to the Mold Surface under the weight of the ring when the assembly is heated for about 1 hour at 2,400 °F (≈1,300 °C).

Micromachining of a Mesoscale Vibratory Gyroscope

High-performance miniature gyroscopes would be fabricated by established micromachining techniques.

NASA's Jet Propulsion Laboratory, Pasadena, California

A micromachining-based fabrication process has been proposed for low-volume production of copies of a mesoscale vibratory gyroscope. The process would include steps of photolithography, metallization, deep reactive-ion etching (RIE), Au/Au thermal-compression bonding, and anodic bonding. In the present state of the art, these process steps are well established and the process as a whole would be considered reproducible.

The basic designs and principles of operation of micromachined vibratory gyroscopes were discussed in several prior *NASA Tech Briefs* articles. For the purpose of the present discussion, the relevant micromachined components of the mesoscale vibratory gyroscope to be fabricated would be a baseplate; a resonator to be mounted on the baseplate; and a post to be affixed to (and thereby become part of) the resonator.

Although the proposed fabrication process would be simple in comparison with some other micromachining processes, it would nevertheless consist of numerous steps and therefore is only summarized here. The baseplate, resonator, and post would be fabricated separately from silicon wafers. The fabrication of the baseplate would include photolithography and etching steps to form pillars to support the resonator; photolithography, metal-evaporation, and liftoff steps to form metal bonding pads and electrical conductors; and photolithography and deep-RIE steps to form through-the-thickness holes. The fabrication of the resonator would include similar but fewer steps (no pillar-formation steps).

The figure depicts the last joining steps. The resonator would be joined to the baseplate by thermal-compression bonding of surface gold layers on their mating metal bonding pads, at a temperature of 350 °C. Top and bottom parts of the post would be joined to the upper and lower surfaces, respectively, of the resonator by anodic bonding at a potential of 4.25±0.25 kV and temperature of ≈400 °C.

This work was done by Kirill Shcheglov of Caltech for **NASA's Jet Propulsion Laboratory**. *For further information, access the Technical Support Package (TSP)* ***free on-line at www.nasatech.com***.

In accordance with Public Law 96-517, the contractor has elected to retain title to this invention. Inquiries concerning rights for its commercial use should be addressed to

Intellectual Assets Office
JPL
Mail Stop 202-233
4800 Oak Grove Drive
Pasadena, CA 91109
(818) 354-2240
E-mail: ipgroup@jpl.nasa.gov

Refer to NPO-30288, volume and number of this NASA Tech Briefs *issue, and the page number.*

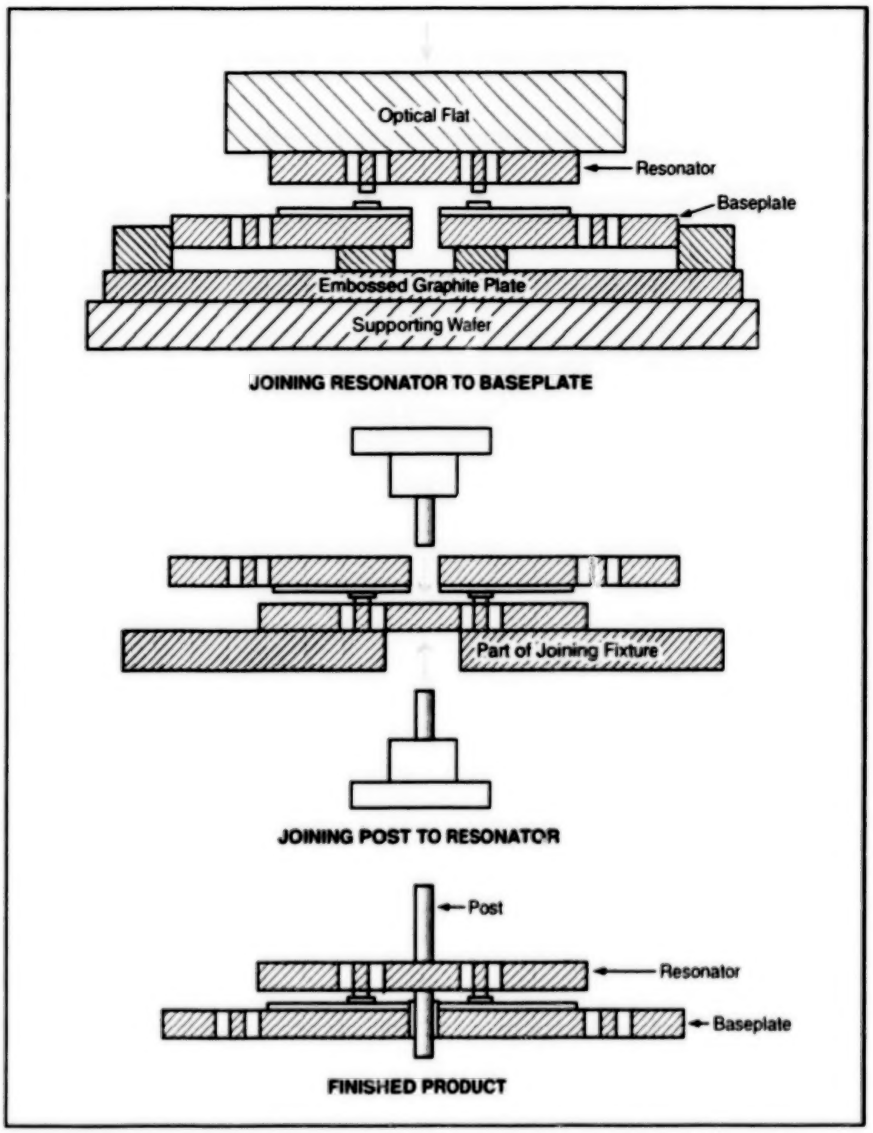

Separately Micromachined Components of a vibratory gyroscope are joined in thermal-compression and anodic-bonding steps.

Mathematics and Information Sciences

Hardware, Techniques, and Processes

47 Coupled-Layer Architecture for Advanced Software for Robots

48 Characteristics of Dynamics of Intelligent Systems

BLANK PAGE

Coupled-Layer Architecture for Advanced Software for Robots

Decision-making and functional infrastructures interact at all levels of granularity.

NASA's Jet Propulsion Laboratory, Pasadena, California

The title "Coupled Layer Architecture for Robotics Autonomy" (CLARATy) refers to a software architecture for robots that has been proposed to (1) improve the modularity of robotic-system software while (2) tightening the coupling between autonomy and control software subsystems. Whereas prior robotic architectures have typically been characterized by three layers, the CLARATy is characterized by only two layers. The CLARATy provides for interaction of decision-making and functional infrastructures at all levels of system granularity. This architecture is flexible enough to encompass research and application domains, and provides for an explicit coupling of artificial-intelligence and robotics techniques. The architecture is also implemented in an object-oriented fashion that makes it possible to leverage software design through both inheritance and aggregation, thereby eliminating the need for duplication of effort in the development of new software.

In a typical three-layer architecture (see figure), the dimension along each layer can be thought of as the breadth of the system in terms of hardware and capabilities. The dimension up from one layer to the next can be thought of as increasing intelligence, from reflexive, to procedural, to deliberative. However, the responsibilities and height of each layer are not strictly defined, and the line between the planner and executive layers can be blurred. Another shortcoming of a typical prior three-layer architecture is lack of access of the planner to the functional layer. While this lack of access is typically desirable during execution, it separates the planner from information on functionality of the system during planning. One consequence is that a planner often carries its own model of the robotic system, which model may not be directly derived from the model carried in the functional layer. This not only entails repetition of information storage but also often leads to inconsistencies. Still another shortcoming of a typical three-layer architecture is that it misrepresents the granularity in the system and obscures the hierarchies that can exist within the three layers.

In the CLARATy, the planner and executive layers are replaced by a single decision layer that performs both planning and executive functions. The CLARATy offers two major advantages over a typical three-layer architecture: explicit representation of the granularity in a third dimension and blending of the declarative and procedural techniques for decision making. The addition of the granularity dimension enables explicit representation of the hierarchies in the functional layer while accounting for the *de facto* nature of planning horizons in the decision layer. For the functional layer, an object-oriented hierarchy describes the nested encapsulation of subsystems of the system and provides basic capabilities at each level of the nesting. For instance, a command to "move" could be directed at a motor, appendage, mobile robot, or team. For the decision layer, granularity maps to an activities time line that is being created and executed. Because of the nature of the dynamics of the physical system controlled by the functional layer, there is a strong correlation between its system granularity and the time-line granularity of the decision layer.

The blending of declarative and procedural techniques in the decision layer emerges from the trend of planning and scheduling systems that have executive qualities and vice versa. This trend has been a cumulative result of recent advances in algorithms for robotic systems and the development of computers capable of processing data at higher speeds. The CLARATy enhances this trend by explicitly providing for access to the functional layer at higher levels of granularity (that is, larger grains), and hence less frequently, thereby providing more time for iterative replanning. However, it is still recognized that there is a need for procedural system capabilities, both in (1) the interface between the executive and functional layers and (2) the infusion of procedural semantics for specifying plans and scheduling operations. Therefore, the CLARATy includes a single database at the interface between planning and executive sublayers, leveraging recent efforts to merge the executive and planner layers.

This work was done by Darren Mutz, Hari Das, Issa Nesnas, Richard Petras, Richard Volpe, and Tara Estlin of Caltech for **NASA's Jet Propulsion Laboratory**. *For further information, access the Technical Support Package (TSP)* ***free on-line at www.nasatech.com***.

This software is available for commercial licensing. Please contact Don Hart of the California Institute of Technology at (818) 393-3425. Refer to NPO-21218.

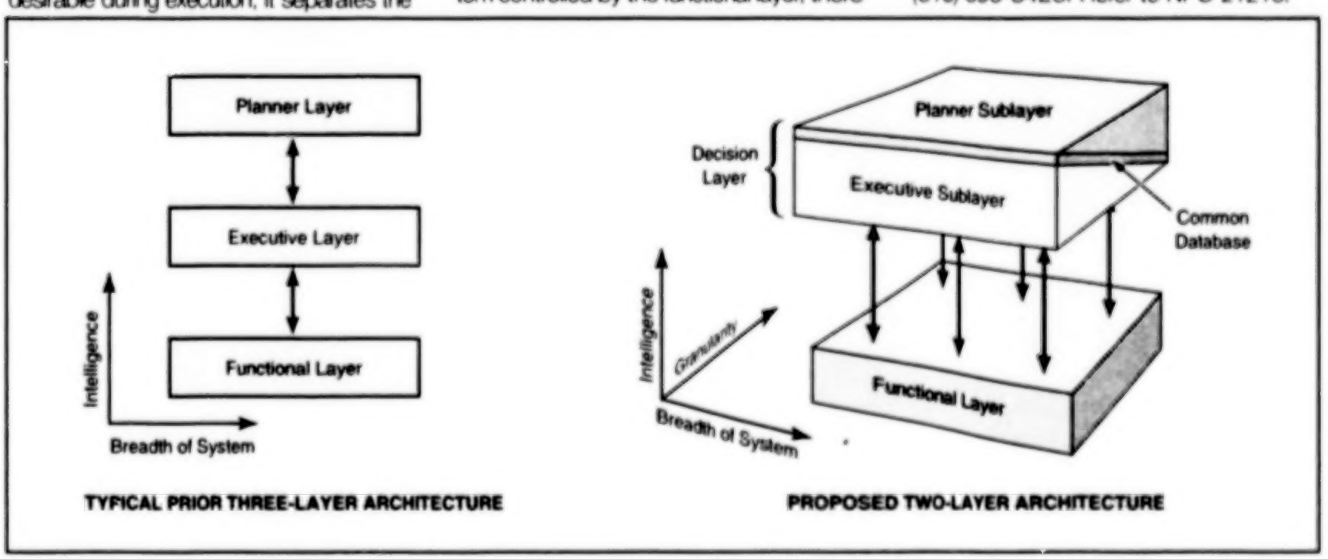

The Decision Layer in the CLARATy performs functions that include (among others) those that, in older three-layer architectures, are performed by separate planner and executive layers.

Characteristics of Dynamics of Intelligent Systems

These characteristics are proposed as means of discriminating between living and nonliving systems.

NASA's Jet Propulsion Laboratory, Pasadena, California

An investigation of nonlinear mathematical models of dynamics has led to the selection of characteristics that could be useful for distinguishing mathematically between the behaviors of (1) intelligent or living systems and (2) nonliving systems. As contemplated here, an intelligent or living system could range from a natural or artificial single-cell organism at one extreme to the whole of human society at the other extreme, whereas a nonliving system could be, for example, a collection of interacting particles or mechanisms. Among other findings, the investigation has revealed that living systems can be characterized by nonlinear evolution of probability distributions over different possible choices of the next steps in their motions.

One of the main challenges in mathematical modeling of living systems is to distinguish between random walks of purely physical origin (for instance, Brownian motions) and those of biological origin. Following a line of reasoning from prior research, it was assumed, in this investigation, that a biological random walk can be represented by a nonlinear mathematical model that represents coupled mental/motor dynamics incorporating the psychological concept of reflection or self-image. The nonlinear dynamics impart the lifelike ability to behave in ways and to exhibit patterns that depart from thermodynamic equilibrium. Reflection has traditionally been recognized as a basic element of intelligence.

In this investigation, the motor dynamics were represented by (1) a generator of stochastic processes representing the motor dynamics of a nonlinear one-dimensional random walk plus (2) a model of the corresponding evolution of the dynamics in probability space. Associated with the probabilistic model of the motor dynamics was a nonlinear version of the Fokker-Planck equation representing the flows of information in probability space: this model was taken to represent both the mental dynamics and a probabilistic self-image of the dynamic system. It was postulated that if the dynamic system "possesses" its self-image, then it can predict future expected values of its parameters and change the expectations if they are not consistent with what is observed.

It was then shown that a living system according to this model can predict the future in terms of probabilities, because of the smoothness of the evolution in probability space (such smoothness does not exist in physical space because of irregularities of a random walk). This ability to predict increases chances for survival and can be considered a basic component of intelligence. It was shown that the coupled motor/mental dynamics can simulate such lifelike phenomena as emerging self-organization, decision-making based on "common sense," predator/prey evolutionary games, and a collective brain. Both the mental and motor dynamics can be implemented by hardware (e.g., neural networks or cellular automata), thereby enabling artificially intelligent systems to exhibit such lifelike phenomena.

This work was done by Michail Zak of Caltech for **NASA's Jet Propulsion Laboratory**. *For further information, access the Technical Support Package (TSP)* ***free on-line at www.nasatech.com***.

NPO-21037

END

01-20-04